2002

Polarized fluorescence depletion reports orientation distribution and rotational dynamics of muscle cross-bridges

Marcus G. Bell
Philadelphia College of Osteopathic Medicine, MarcusBe@pcom.edu

Robert E. Dale

Uulke A. Van Der Heide

Yale E. Goldman

Polarized Fluorescence Depletion Reports Orientation Distribution and Rotational Dynamics of Muscle Cross-Bridges

Marcus G. Bell,* Robert E. Dale,*† Uulke A. van der Heide,*‡ and Yale E. Goldman*

*Pennsylvania Muscle Institute, The School of Medicine, University of Pennsylvania, Philadelphia, Pennsylvania 19104-6083; †King's College London, London SE1 1UL, England; and ‡Universitair Medisch Centrum Utrecht, The Netherlands

ABSTRACT The method of polarized fluorescence depletion (PFD) has been applied to enhance the resolution of orientational distributions and dynamics obtained from fluorescence polarization (FP) experiments on ordered systems, particularly in muscle fibers. Previous FP data from single fluorescent probes were limited to the 2nd- and 4th-rank order parameters, $\langle P_2(\cos\beta)\rangle$ and $\langle P_4(\cos\beta)\rangle$, of the probe angular distribution (β) relative to the fiber axis and $\langle P_{2d}\rangle$, a coefficient describing the extent of rapid probe motions. We applied intense 12-μs polarized photoselection pulses to transiently populate the triplet state of rhodamine probes and measured the polarization of the ground-state depletion using a weak interrogation beam. PFD provides dynamic information describing the extent of motions on the time scale between the fluorescence lifetime (e.g., 4 ns) and the duration of the photoselection pulse and it potentially supplies information about the probe angular distribution corresponding to order parameters above rank 4. Gizzard myosin regulatory light chain (RLC) was labeled with the 6-isomer of iodoacetamidotetramethylrhodamine and exchanged into rabbit psoas muscle fibers. In active contraction, dynamic motions of the RLC on the PFD time scale were intermediate between those observed in relaxation and rigor. The results indicate that previously observed disorder of the light chain region in contraction can be ascribed principally to dynamic motions on the microsecond time scale.

INTRODUCTION

A plausible hypothesis for the production of force in the actomyosin system is the lever arm model which proposes that, during the energy transducing cycle, the motor domain (MD) of the myosin head binds rigidly to actin in the thin filament, and a hinge within the myosin head allows the light chain domain (LCD) to tilt like an arm flexing at its elbow (Huxley and Kress, 1985; Cooke, 1986; Vibert and Cohen, 1988; Rayment et al., 1993a; Goldman, 1998; Geeves and Holmes, 1999). The crystal structure of chicken skeletal myosin subfragment 1 (S1) (Rayment et al., 1993b) provided strong support for this hypothesis and stimulated many experiments designed to detect tilting motions of myosin domains.

Relative motion between the catalytic and light chain domains during the ATPase cycle of myosin fragments has been detected from electric birefringence (Highsmith and Eden, 1986), scattering of x-rays and neutrons (Wakabayashi et al., 1992; Mendelson et al., 1996), electron paramagnetic resonance (EPR) of spin labels (Adhikari et al., 1997), resonance energy transfer (Suzuki et al., 1998; Shih et al., 2000) and comparison of crystal structures with various bound nucleotide and phosphate analogs (Fisher et al., 1995; Smith and Rayment, 1996; Dominguez et al., 1998; Houdusse et al., 1999). These studies have shown that the MD and LCD rotate relative to each other as expected for a lever arm mechanism. In the transition state between M · ATP and M · ADP · P_i, the myosin head is bent with the LCD tilted toward the ATP binding site. Upon release of P_i from M · ADP · P_i, myosin straightens by rotation of the LCD together with part of the motor domain, termed the converter, relative to the rest of the MD. Based on the orientation of myosin with respect to actin in decorated actin filaments (Rayment et al., 1993a; Milligan and Flicker, 1987), the straightening of S1 tilts the LCD in a direction that would actively move the load (thick filament or cargo) toward the barbed end of actin (Z line in muscle). This "power stroke" is reversed during the hydrolysis step M · ATP to M · ADP · P_i or at an isomerization just before this step (Suzuki et al., 1998). These studies were all conducted on fragments of myosin bearing no mechanical force, and most of them in the absence of actin. Thus, the relationship between the conformational changes of isolated myosin and tilting motions in an active muscle fiber is still unclear. In particular, does the tilting of the light chain accompany force generation, filament sliding or both? Does the MD rotate relative to actin as well? These questions can be addressed only by experiments on systems actually transducing chemical energy to mechanical work.

Structural biological methods have been applied to detect tilting motions of myosin domains in muscle fibers. In low-angle x-ray diffraction patterns of muscle, the intensity and splitting of the 14.3-nm meridional reflection are sensitive indicators and provide strong support for tilting and flexibility of the LCD (Huxley et al., 1983; Lombardi et al., 1995; Dobbie et al., 1998; Linari et al., 2000). Fluorescent probes and extrinsic spin labels have been placed in the motor domain at a highly reactive thiol, Cys^{707}, of the rabbit

Submitted October 23, 2001, and accepted for publication April 25, 2002.

Address reprint requests to Yale E. Goldman, D700 Richards Bldg., 3700 Hamilton Walk, Philadelphia, PA 19104-6083. Tel.: 215-898-4017; Fax: 215-898-2653; E-mail: goldmany@mail.med.upenn.edu.

Dr. Marcus Bell's current address is Philadelphia College of Osteopathic Medicine, Philadelphia, PA 19131.

0006-3495/02/08/1050/24 $2.00

psoas myosin heavy chain (Borejdo et al., 1982; Tanner et al., 1992; Berger et al., 1996; Cooke et al., 1982; Hellen et al., 1995), and at various positions in the RLC (Hambly et al., 1992; Irving et al., 1995, Ling et al., 1996; Allen et al., 1996; Sabido-David et al., 1998; Corrie et al., 1999, Hopkins et al., 2002). Electron microscopy also resolved the MD and LCD (Pollard et al., 1993; Taylor et al., 1999).

These studies have generally shown that both the MD and the LCD have a broad orientation distribution in relaxation and contraction and a narrower distribution in rigor. During contraction, the ordered component of the MD hardly tilts in response to perturbations that alter tension, such as length steps (Cooke, 1981; Berger et al., 1996; Burghardt et al., 1997) or increase of phosphate concentration (Zhao et al., 1995), suggesting that it is rigidly attached to actin. However, some evidence suggests that the MD does rotate during force development (Taylor et al., 1999; Tsaturian et al., 1999). The LCD tilts in response to applied length changes (Irving et al., 1995; Hopkins et al., 1998; Dobbie et al., 1998; Corrie et al., 1999), providing further support for the lever arm hypothesis for contraction of the fully assembled sarcomere.

The angular distributions for relaxed and actively cycling heads may be broad due to dynamic motions from thermal reorientation on the nanosecond to microsecond timescale or sequential population of the states of the enzymatic cycle up to the millisecond timescale. Additional static disorder is expected among the attached myosin heads, due to the incommensurate periodicities of the actin and myosin filaments (Huxley and Brown, 1967).

Time-resolved decay of phosphorescence anisotropy (TPA) and saturation transfer EPR (ST-EPR) are capable of detecting protein rotational dynamics on the microsecond time scale of the cross-bridge motions expected in an active muscle fiber. These techniques have been applied to muscle fibers and myofibrils labeled at Cys^{707} (Thomas et al., 1980; Barnett and Thomas, 1984, 1989; Ludescher and Thomas, 1988; Stein et al., 1990; Berger and Thomas, 1993) and have identified components of motion of the MD at approximately 20 and 300 μs that are unique to active contractions (Stein et al., 1990). However, few reports of ST-EPR or TPA have been carried out with probes bound to sites on the RLC (Thomas et al., 1995; Ramachandran and Thomas, 1999). ST-EPR reports the time scale of motions but cannot independently resolve the amplitude. TPA is somewhat insensitive because the phosphorescence emission is $\sim 10^5$-fold dimmer than fluorescence (Johnson and Garland, 1981; Yoshida and Barisas, 1986).

Here we report the development of a novel extension of fluorescence polarization spectroscopy on ordered samples, such as muscle fibers, to resolve the extent of dynamic motions on the 20- to 500-μs time scale with improved sensitivity. Polarized fluorescence depletion (PFD) has been described for isotropic samples, membranes and cells (Johnson and Garland, 1981; Yoshida and Barisas, 1986; Corin et al., 1987; Londo et al., 1993). Hellen et al. (1995) have used a similar method to detect motions of probes bound to Cys^{707} in muscle fibers.

In the absence of oxygen, fluorescent probes will often populate a long-lived triplet state. Triplet population is not restricted to probes exhibiting phosphorescence emission. Following transient pumping of probes into the triplet state, the probes remaining in the ground state have an orientational distribution that is depleted around the polarization direction of the pumping pulse. This polarized depletion is detected by fluorescence excited by a weak interrogation beam, and it lasts until it is filled in by dynamic rotational motions and decay of the triplet population. The PFD method potentially provides dynamic information describing the extent of motions on the time scale between the fluorescence lifetime (one to a few ns) and the duration (up to a few ms) of the triplet state as well as improved detail about the static probe orientation. As implemented here, using rhodamine as the probe, the PFD technique provides a practical, sensitive method to detect the dynamics of protein rotational motions in the time scale 4 ns $\ll t \ll$ 20 μs.

The PFD technique was used in the present work to determine the orientation and mobility of the myosin LCD in single muscle fibers in relaxation, contraction, and rigor. During contraction, motions of the RLC on the microsecond time scale are sufficient to account for much of the orientational dispersion. Part of the work has previously been reported in abstract form (Bell et al., 2000).

THE THEORY OF PFD

Polarized fluorescence depletion is an enhancement of fluorescence polarization that enables characterization of the orientation distribution of fluorescent probes in an ordered system at higher resolution than either fluorescence or phosphorescence polarization. It can provide information on the rate and extent of rotational motions on a time scale comparable with that of the decay of phosphorescence (Johnson and Garland, 1981; Yoshida and Barisas, 1986; Dale, 1987; Corin et al., 1987).

In an ordered biological system such as a biological membrane or a muscle fiber, specifically labeled with an extrinsic fluorophore, an intense pulse of exciting light is applied to the probe. A proportion of the optically excited chromophores undergoes intersystem crossing to populate a long-lived triplet excited state, temporarily leaving a reduced population of probes in the ground state. This pulse excitation of the triplet state is termed transient bleaching or photoselection. Several factors govern the angular distribution of the probes remaining in the ground state for a period, typically several milliseconds, after the photoselection pulse: 1) the angular distribution of the population that was present before the bleaching pulse; 2) the polarization of the bleaching pulse; 3) the extent of bleaching; 4) the rate of

return to the ground state of the triplet population; and 5) rotational motions of the probe reflecting those of the labeled proteins. Polarized fluorescence of the ground state population is detected using a weak excitation beam to interrogate the same sample volume.

Relationships involving the steady-state polarized fluorescence intensities before and the diminished intensities after the photobleaching pulse are derived in the Appendix, which shows how the orientation distribution and dynamics can be determined. The bleached population has an orientation distribution that initially corresponds to a convolution of the original steady-state distribution with the angular distribution of bleaching efficacy. Differences of polarized intensities of fluorescence before and after the bleaching pulse yield estimates of the orientation distribution and dynamics of this bleached population. The distribution of the bleached population relaxes toward the steady-state distribution by rotational motions detectable in the time range greater than the fluorescence lifetime (e.g., 4 ns) and up to several lifetimes of the triplet state. Such rotations cause ratios of the polarized difference intensities to decay toward those of the pre-bleach fluorescence. Finally, in the absence of irreversible bleaching, the difference intensities decay to zero due to return of the excited triplet population to the ground state.

Probes useful in PFD should have triplet lifetimes similar to or longer than the protein rotations of interest, but they need not exhibit delayed luminescence (phosphorescence or delayed fluorescence). The fluorescent probe used here, rhodamine, has a fluorescence (singlet excited state) lifetime, τ_f, of ~4 ns, and exhibits no appreciable phosphorescence under the conditions of the present studies.

The probability of absorption of a photon by a probe is proportional to $\cos^2 \theta_a$, where θ_a is the angle between the electric vector of the linearly polarized excitation beam and the probe absorption dipole moment. The probability of detecting a photon through an analyzing polarizer is given by $\cos^2 \theta_e$, where θ_e is the angle between the electric vector of the emitted photon transmitted by the analyzer and the probe emission dipole moment. Thus, in a standard steady-state fluorescence polarization experiment, the polarized fluorescence intensity is given by:

$$ {}_{E}I_{E'} = I_0\langle (E \cdot a)^2 (E' \cdot e)^2 \rangle \qquad (1) $$

where I_0 represents the total fluorescence intensity, independent of polarization, E denotes the polarization of the excitation beam, E' that of the detected component of the emitted beam, and a and e denote unit vectors representing the absorption and emission dipoles for a single chromophore. The brackets, $\langle\ \rangle$, denote an ensemble average taken by integrating the probability density functions for a and e over all spherical angles.

Using measurements of ${}_{E}I_{E'}$ with excitation and emission polarizations parallel and perpendicular to the muscle fiber axis, F, and optical paths perpendicular to that axis, three order parameters describing the probe orientation distribution are obtainable: $\langle P_{2d} \rangle$, $\langle P_2 \rangle$ and $\langle P_4 \rangle$ (Dale et al., 1999; Hopkins et al., 2002; see Appendix). The order parameters are coefficients of a series expansion describing the orientation distributions using the Legendre polynomials as basis functions (Dale et al., 1999; see Appendix). $\langle P_{2d} \rangle$ describes the extent of subnanosecond rotational motions (wobble) of the probe transition dipoles about an axis, c, defined relative to the protein structure and $\langle P_2 \rangle$ and $\langle P_4 \rangle$ describe the orientation distribution of c relative to F. Both static disorder of c and dynamic disorder caused by motions that are slower than the probe's fluorescence lifetime, τ_f, contribute to determining $\langle P_2 \rangle$ and $\langle P_4 \rangle$. The effect of fast probe motions, however, has been 'factored out' of $\langle P_2 \rangle$ and $\langle P_4 \rangle$ (Appendix Eqs. D.15 and D.16). The description used here makes the assumption that the absorption and emission dipoles are collinear, as approximately applies for rhodamine (Chen and Bowman, 1965; Penzkofer and Wiedmann, 1980; Hopkins et al., 1998), but the case of probes with non-collinear dipoles can be analyzed in similar terms (Londo et al., 1993; Dale et al., 1999).

In a PFD experiment, additional orientation and dynamic information becomes available because correlation between three photons (photoselection, interrogation and emission) combine to determine the polarization. As shown in the Appendix, if the extent of transient photobleaching is low, the difference, Δ, between intensities measured before and after a transient photoselection pulse is given by an expression similar to Eq. 1,

$$ {}_{`E,E}\Delta_{E'} = I_0 B\langle (`E \cdot b)^2 (E \cdot a)^2 (E' \cdot e)^2 \rangle \qquad (2) $$

where B is a scale factor proportional to the extent of bleaching, $`E$ is the polarization vector of the photoselection pulse and b is the orientation of the absorption dipole at the instant of bleaching (Appendix, Fig. A.1).

Let order parameters $\langle P_{2p} \rangle$ and $\langle P_{4p} \rangle$ describe rotational motions of c on an intermediate (microsecond) time scale longer than the fluorescence lifetime (τ_f) but still much shorter than the time, τ_p, between application of the bleaching pulse and measurement of the remaining fluorescence ($\tau_f \ll \tau \ll \tau_p$). These order parameters are analogous to $\langle P_{2d} \rangle$ for fast wobble ($\tau \ll \tau_f$). Just as $\langle P_{2d} \rangle$ is found from measurements of ${}_{E}I_{E'}$, $\langle P_{2p} \rangle$ and $\langle P_{4p} \rangle$ can be estimated from measurements of ${}_{`E,E}\Delta_{E'}$ with various combinations of polarizer orientations and optical paths. $\langle P_{2p} \rangle$ and $\langle P_{4p} \rangle$ are determined by the extent of rotational motions of c (defined above) on the intermediate time scale about a slower-moving axis, p, also defined within the protein. Defining order parameters, $\langle P_{2s} \rangle$, $\langle P_{4s} \rangle$ and $\langle P_{6s} \rangle$, for the static orientation distribution of p with the microsecond wobble parameters "factored out," then:

$$ \langle P_2 \rangle = \langle P_{2p} \rangle \langle P_{2s} \rangle $$

$$ \langle P_4 \rangle = \langle P_{4p} \rangle \langle P_{4s} \rangle \qquad (3) $$

The Appendix describes how $\langle P_{2p}\rangle$, $\langle P_{4p}\rangle$, $\langle P_{2s}\rangle$, $\langle P_{4s}\rangle$ and $\langle P_{6s}\rangle$ can be determined from experimentally measured intensities ($_{E}I_{E'}$) and intensity differences ($_{E,E}\Delta_{E'}$), thereby separating microsecond ($\tau_f \ll \tau \ll \tau_p$) wobble from static disorder and/or any motions of p on a slower time scale than that of triplet decay. Both static disorder of p and dynamic disorder caused by motions that are slower than τ_p contribute to determining $\langle P_{2s}\rangle$, $\langle P_{4s}\rangle$ and $\langle P_{6s}\rangle$. Thus the PFD method extends the time scale of motions detectable by fluorescence polarization and potentially provides extra resolution (up to $\langle P_{6s}\rangle$) of the orientation distribution static on that time scale.

The above description applies to a situation in which the intensity of the photoselection pulse is low enough that the probability of bleaching a particular probe molecule is $B\cos^2\theta_b$, where θ_b is the angle between the polarization of the photoselection pulse and the probe absorption dipole moment, B is the depth of bleaching, and Eq. 2 is applicable. Most of the experiments presented in this paper were analyzed under this low-bleach assumption. Unlike in a standard (non-bleaching) fluorescence experiment, however, the photoselection pulse can be intense enough that, for probes at orientations close to its polarization vector, bleaching becomes partially saturated and no longer proportional to intensity (Axelrod et al., 1976; Hellen and Burghardt, 1994). The full expression for the angular dependence of the probability of bleaching, due to a linearly polarized beam of uniform intensity, is $1 - \exp(-B(\mathbf{E}\cdot\mathbf{b})^2)$ (Dale, 1987), rather than $B(\mathbf{E}\cdot\mathbf{b})^2$. The results of experiments using a range of bleach amplitudes can be used to check the validity of assuming the simpler low-bleach angular dependence, $B(\mathbf{E}\cdot\mathbf{b})^2$. Expressions that apply to the high-bleach regime and used for this validity check are listed in the Appendix. In principle, higher-rank order parameters (e.g. $\langle P_{8s}\rangle$) can also be obtained with deep bleaching, but measurement uncertainties limit the practicability of extending the analysis beyond the 6th rank.

MATERIALS AND METHODS

Chemicals and solutions

Solution compositions were as described in Hopkins et al. (1998). Nucleotides and rabbit skeletal muscle troponin were obtained from Sigma (St. Louis, MO). The 6-isomer of iodoacetamidotetramethylrhodamine (6-IATR) was kindly provided by Dr. John Corrie, synthesized as previously described (Corrie and Craik, 1994). Chicken gizzard wild-type regulatory light chain was expressed in *Escherichia coli*, purified, and labeled at its native cysteine residue (108) with the 6-IATR (Sabido-David et al., 1998). Troponin C was prepared as described by Dobrowolski et al. (1991) with modifications.

Muscle fiber preparation and RLC exchange

In preparation for the experiment, 4-mm segments of single muscle fibers were dissected from glycerinated bundles of rabbit psoas muscle (Goldman et al., 1984). Fiber ends were held in aluminum foil T-clips, and the sarcomeres inside and within 100 μm of the T-clips were cross-linked by glutaraldehyde (Allen et al., 1996). The fiber segment was then mounted in the experimental apparatus in 5 mM MgATP relaxing solution at 11°C, and activated briefly (as described below) to test integrity of the fiber. Length and cross-sectional area were measured (Goldman and Simmons, 1984).

Regulatory light chain, monofunctionally labeled with rhodamine at Cys^{108}, was exchanged for native RLC as described previously (Ling et al., 1996). Briefly, the fiber was incubated for $\geq$2 min each in relaxing solution containing 0.1 mM MgATP ("0.1 Rel") at 10°C, rigor solution at 10°C, exchange solution at 10°C, and then for 30 min at 30°C in exchange solution containing 0.5 mg/ml labeled RLC and to which 3 mM DTT had been freshly added. The fiber then was cooled quickly to 10°C and relaxed in relaxing solution containing 5 mM MgATP ("5 Rel"). Troponin and troponin C extracted during RLC exchange were replenished by incubation for 40 min at 10°C in 5 Rel containing 0.5 mg/ml troponin then for 10 min in 5 Rel containing 0.5 mg/ml troponin C. Following the exchange procedure, active tension at 11°C was 0.94 $\pm$ 0.28 (mean $\pm$ S.D., $n = 6$) of that before exchange, consistent with previous results (Ling et al., 1996, Allen et al., 1996). Due to a thermal gradient, the solution trough in which fiber mechanical and spectroscopic parameters were assayed was about one degree higher than the other troughs.

Experimental apparatus

Optical system

The labeled muscle fiber was held in a mechanical setup, similar to that described by Goldman et al. (1984) and Hopkins et al. (1998), that allowed switching of the bathing medium and monitoring of force and polarized fluorescence intensities. The optical arrangement for PFD experiments is shown in Fig. 1. The geometry is similar to that described by Hopkins et al. (1998) and Allen et al. (1996), but with additional components related to the PFD transient bleaching protocol.

An argon ion laser (Coherent model Innova 90-5), emitting 1.4 W at $\lambda = 514.5$ nm in optical servo mode, was used to apply both the photoselection (bleaching) pulses and the weaker fluorescence interrogation beams to the same volume of the sample. An acousto-optical (AO) diffraction modulator (model 8873, NEC) controlled the intensity. A telescope comprising 70 and 35 mm achromatic doublet lenses (Edmund Scientific, Barrington, NJ) concentrated and steered the laser beam into the AO crystal slightly off of the optical axis of the setup so that the emergent first order beam scattered by the acoustic waves was aligned with the optical axis. The intensity modulated diffracted beam was selected by an iris diaphragm and polarized vertically by a polarizing beamsplitting cube (BBPC12-550, Karl Lambrecht, Chicago, IL). A small fraction of the excitation beam was reflected by a glass coverslip to a photodiode with integral 514 nm interference filter (42-5231-01, Ealing Optical, Ltd., Watford, UK) to monitor the intensity. The main beam was passed through a 250-mm focal length achromatic relay lens into a Pockels cell (ammonium dihydrogen phosphate, model 370, Conoptics Inc., Danbury, CT) that modulated its polarization. The principal (slow) axis of the Pockels cell crystal was tilted 45° from vertical. A laboratory-built high voltage amplifier applied a -100 V to $+250$ V electrical potential across the crystal, tuned to retard the component of incident light polarized along its slow axis by 0 or $\lambda/2$ relative to the component on the fast axis. This voltage control switched the laser polarization (within 2 μs) between vertical (perpendicular to the muscle fiber axis) and horizontal (parallel to the fiber axis). The extinction by crossed polarizers was typically >200-fold. Between experimental trials, a mechanical shutter (Uniblitz, Vincent Associates) blocked the laser light.

The intensity- and polarization-modulated beam was passed through a 514 nm, 10 nm FWHM interference filter (Omega Optical) to block long wavelengths from the pumping arc in the laser cavity. A solenoid-driven, rotating mirror (fabricated in-house) directed the excitation beam along either a vertical (x) or horizontal (y) path to the fiber. Achromatic lenses of 35 mm focal length

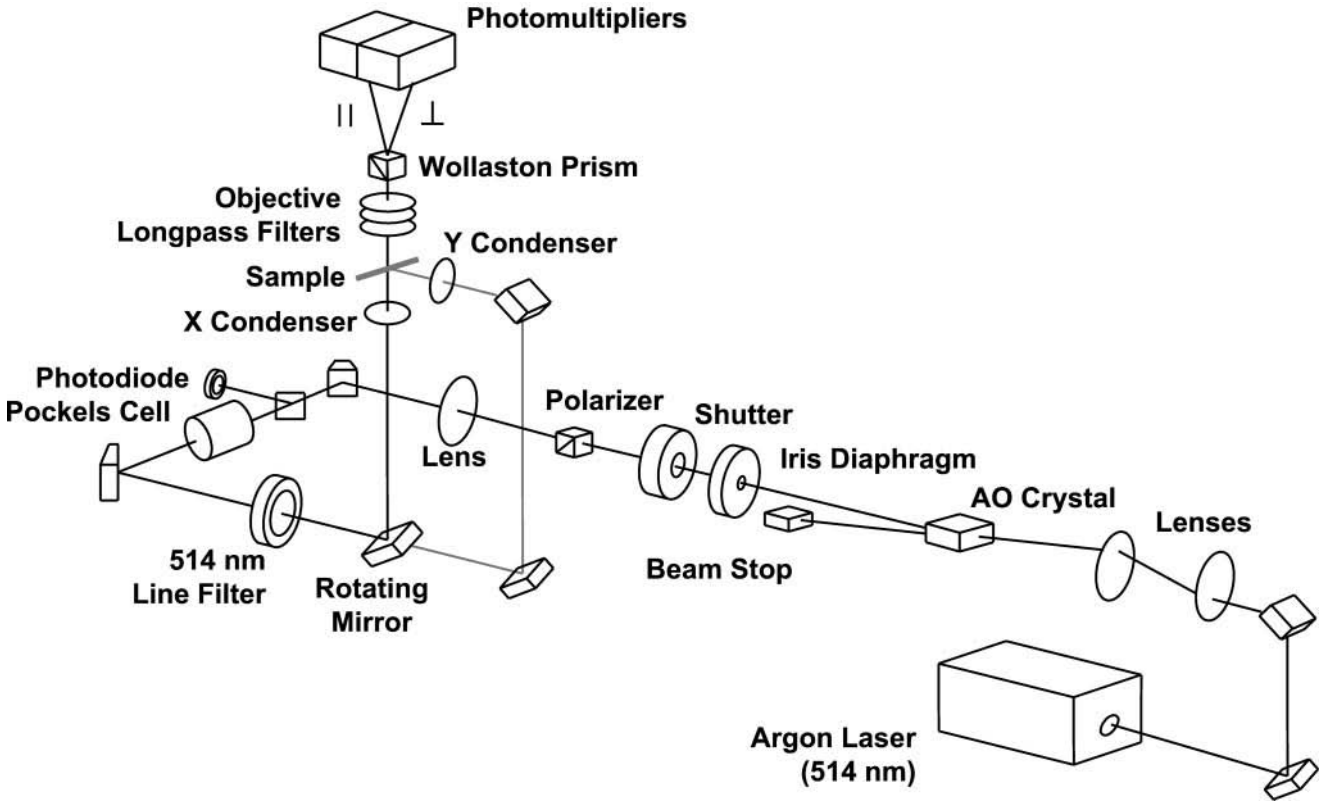

FIGURE 1 Experimental apparatus. Schematic diagram of the optics for pulsed photoselection and interrogation of fluorescence depletion. The sample is a solution of rhodamine, a PVA film containing rhodamine or a muscle fiber held in a trough containing an aqueous solution. The acousto-optic (AO) deflector, shutter, Pockels cell, rotating mirror and photomultiplier gating are under computer control.

in focusing mounts served as condensers. The laser beam diameter entering the condensers was 2 mm, and the optics were adjusted so that the x and y excitation beams illuminated the same 0.2 mm diameter spot at the fiber, which was positioned slightly beyond the beam focus.

Fluorescence was collected through a 1 cm path length fused silica cuvette containing 100 mM $K_2Cr_2O_7$ and then a Schott glass 590 nm long-pass filter. The purpose of the $K_2Cr_2O_7$ liquid filter was to block the 514 nm excitation beam and thus avoid exciting luminescence of the glass filter. A 25 mm diameter, 50 mm focal length achromatic doublet beyond the filters served as an objective lens. The collected light was split into linearly polarized components parallel and perpendicular to the fiber axis by a Wollaston prism (W2A-12-20, Karl Lambrecht). The two emission polarizations were simultaneously detected by two photomultiplier tubes (R4632, Hamamatsu Corp., Bridgewater, NJ), gated as described below.

Electronics and data collection

Timing of the optical switching and signal recording was controlled by a programmable sequence generator. Digital pulses from the sequence generator drove analog interfaces to the AO modulator, mechanical shutter, Pockels cell, $x - y$ switching mirror, photomultiplier gating circuits, and recording oscilloscope. The photobleaching pulse was always polarized parallel to the fiber axis. Polarization of the weaker interrogation excitation beam was alternated between parallel and perpendicular to the fiber axis every 20 μs during recording. The phase of alternation relative to the timing of the photobleaching pulse was selectably alternated by a control input from the sequencer.

Transistorized high-voltage ladder networks were constructed in-house to clamp the photomultiplier dynode potentials and enhance detector linearity (Takeuchi and Nagai, 1985; Kume, 1994). The PMTs were attenuated during the intense photobleaching pulse by electronically swapping the potentials at the photocathode and first dynode (Ballard, 1983; Kao and Verkman, 1996). When gated off, the detector sensitivity was attenuated $>$1000-fold. The photobleaching pulse lasted 12 μs during a blanking interval of 60 μs. The PMTs were switched on 12 μs after the bleaching pulse ended and reached full sensitivity within 2–4 μs with no appreciable further transients (see Figs. 3 *B* and 9). An additional period of 10 μs was allowed before samples were used for analysis to guard against residual PMT gating artifacts. Thus the "dead time" between the end of the photobleaching pulse and analyzed samples was 20–24 μs. The dynode and gating circuits are available on request (from Y.E.G.).

Experimental fiber force, fluorescence intensity, excitation intensity, and timing signals were recorded at 12-bit resolution and 2-μs sampling intervals by a digitizing oscilloscope (model Pro 40, Nicolet Instruments, Madison, WI). To conserve space in its data buffer, the oscilloscope was clocked externally only when the shutter was open and after the $x - y$ mirror had stabilized. The pulses to the AO modulator, $x - y$ mirror, Pockels cell, oscilloscope recording gate and from the photodiode intensity monitor were summed at an oscilloscope input in a way that allowed their decomposition by analysis software off line. The oscilloscope sweep was ended after recording 10 cycles of all combinations of the input directions and polarizations, and the acquired data were transferred through an IEEE-488 interface to a PC.

Experimental protocol

At the beginning of the experiment, the Pockels cell driving voltages were tuned to optimize extinction through vertical and horizontal polarizers,

thereby compensating for any drift of the optical retardation. Spectroscopic reference samples were then assayed as a measure and verification of instrument parameters. The reference samples and their analysis are described later.

A muscle fiber segment was mounted into the experimental apparatus in relaxing solution, tested and measured as described earlier and exchanged with labeled RLC. Spectroscopic trials were then performed in each of the relaxed, rigor, and Ca^{2+}-activated conditions. Several locations along the middle third of the fiber length were assayed for each condition. The ordering of the conditions was randomized to minimize systematic effects of fiber rundown on the spectroscopic data for each condition.

Prior to each rigor contraction, the fiber was incubated for ≥2 min in 0.1 Rel. After PFD signals were recorded for the rigor condition, the fiber was relaxed in 5 Rel. Isometric activation was preceded by incubation for ≥2 min in pre-activating solution containing 0.1 mM EGTA. The fiber was transferred to activating solution containing ~30 μM free Ca^{2+}, and PFD signals were recorded. The fiber was then relaxed in 5 Rel.

The triplet lifetime is highly sensitive to quenching by oxygen in the solutions (Calhoun et al., 1983), so the relaxing, rigor, and activating solutions were maintained under a stream of argon gas. On the day of each experiment, an oxygen scavenging system of glucose, glucose oxidase and catalase (Calhoun et al., 1983) was added to these solutions. Jets of argon gas were also directed at the fiber solution trough to reduce the surrounding oxygen tension and to eliminate condensation on the optical windows of the trough.

At the end of each experiment, spectroscopic reference samples were again assayed to measure and verify instrument parameters.

Spectroscopic reference samples

Three fluorescent reference samples were fashioned to provide predictable physical and optical properties. The samples were made by sandwiching viscous or solid fluorescent material between two isosceles 45° − 90° − 45° prisms to form a 10-mm cube (Hopkins et al., 1998). The cubes could be placed at the position of the fiber in the experimental setup with faces perpendicular to all of the optical beams. Diffusion of oxygen in the reference samples was inhibited by the viscosity of the solution or the polymer.

A random, viscous solution of IATR was made by diluting a 10 mM stock of IATR in dimethyl formamide into glycerol to 100 μM final concentration. Argon gas was gently bubbled through the solution to mix the dye and to displace dissolved oxygen. The isosceles prisms were held together by strips of double-sided adhesive tape with a gap forming a chamber on the diagonal plane between the prisms. The probe solution was introduced into this gap and the chamber was then sealed with nail polish.

Rigid samples were made from IATR in a polyvinyl-alcohol (PVA) film matrix. PVA powder was dissolved at 1 g/ml in H_2O at 80°C, then maintained at 40°C while IATR stock (10 mM in DMF) was gently stirred in to 20 μM final concentration. Drops of warm PVA-IATR solution were put onto glass slides, which were cured under vacuum to form a ~150-μm-thick film. This film was reannealed at 80°C for 4 h, trimmed to 10 × 5 mm and fixed between two of the 10-mm isosceles prisms with optical grade epoxy (type 302, Epo-tek Corp., Billerica, MA).

Rigid, partially oriented fluorescent samples were made by slowly stretching PVA strips ~5-fold at 80°C using a motor-driven leadscrew. A stretched sample was oriented in the optical cube so that when positioned in the experimental setup, the direction of stretch was oriented along the same axis (*z*) as the muscle fibers. Starting with a somewhat thicker film for stretched samples yielded a final thickness and fluorescence intensity very similar to that of the isotropic (unstretched) PVA sample.

Protocol for polarized fluorescence depletion

At the beginning of each polarized fluorescence depletion (PFD) trial, the mechanical shutter was opened and steady-state fluorescence intensity data

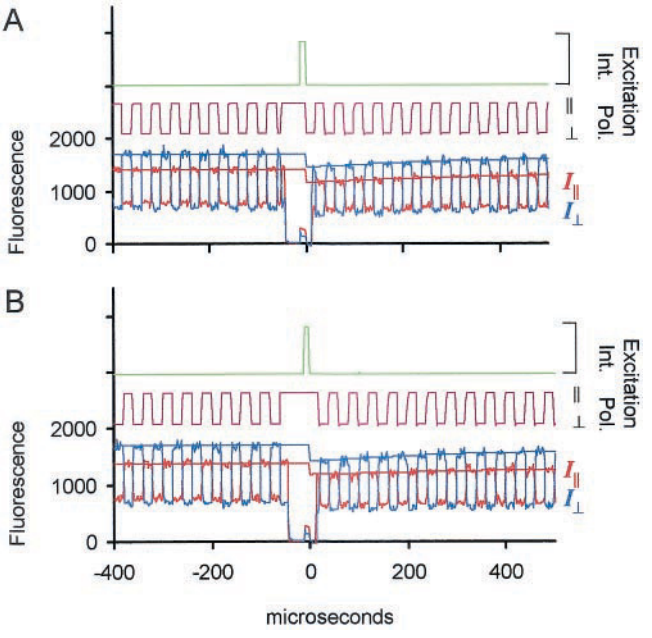

FIGURE 2 Unprocessed data from a single polarized fluorescence depletion (PFD) trial for *x* (in-line) illumination, covering the period before and after the bleach event. The sample is a single muscle fiber in the rigor condition, into which 6-ATR-labeled myosin regulatory light chain had been exchanged. (*A*) At the beginning of the trial, steady-state intensity data were collected for each polarization of fluorescence (*noisy red and blue traces*), in response to alternating excitation polarization (*magenta trace*). For the bleach, excitation (*green trace*) was modulated to high intensity for a 12-μs period ending at time 0, then returned to a lower interrogation setting. *Smooth red and blue lines*: the average of steady pre-bleach fluorescence data, followed by a single exponential fitted to the post-bleach recovery, corresponding to the $_{\parallel}I_{\parallel}$ (red) and $^{x}_{\perp}I_{\parallel}$ (*blue*) components of fluorescence. (*B*) The same as *A*, but during the subsequent trial in which alternation of the excitation polarization was 180° out of phase with respect to that in *A*.

for both emission polarizations were recorded for 200 or 400 μs at a sampling rate of 2 μs. During this period, polarization of the excitation was alternated between parallel and perpendicular to the muscle fiber axis every 20 μs (Fig. 2). Excitation intensity was set to elicit strong fluorescence without causing significant population of the triplet state or irreversible bleaching. This is the "interrogation intensity," as discussed further in the Results section. The photomultipliers (PMTs) were gated off (at −50 μs in Fig. 2) and then the AO modulator increased the intensity (~500-fold) for 12 μs to transiently populate the probe triplet state. The AO modulator then returned the excitation to the interrogation level. During the photoselection pulse, the highly attenuated PMTs responded slightly to the prompt sample fluorescence, giving rise to the small upward deflections ending at time 0 in Fig. 2. The photoselection pulse was polarized parallel to the fiber axis.

After the photoselection pulse, the PMTs were switched back on and fluorescence was recorded for 1.6 ms while the excitation polarization was alternated again every 20 μs. The laser beam was then shuttered off and the data sampling clock was stopped. The sample was kept in the dark for approximately 10 triplet lifetimes to allow complete return to the ground state before the next trial. During that dark time, the data sampling clock was briefly triggered to acquire several data points as a zero-light reference, and the solenoid mirror was switched between *x* and *y* illumination in preparation for the next trial.

After each bleaching pulse, fluorescence detected at the interrogation level was diminished, and it recovered at the rate of triplet decay. In Fig.

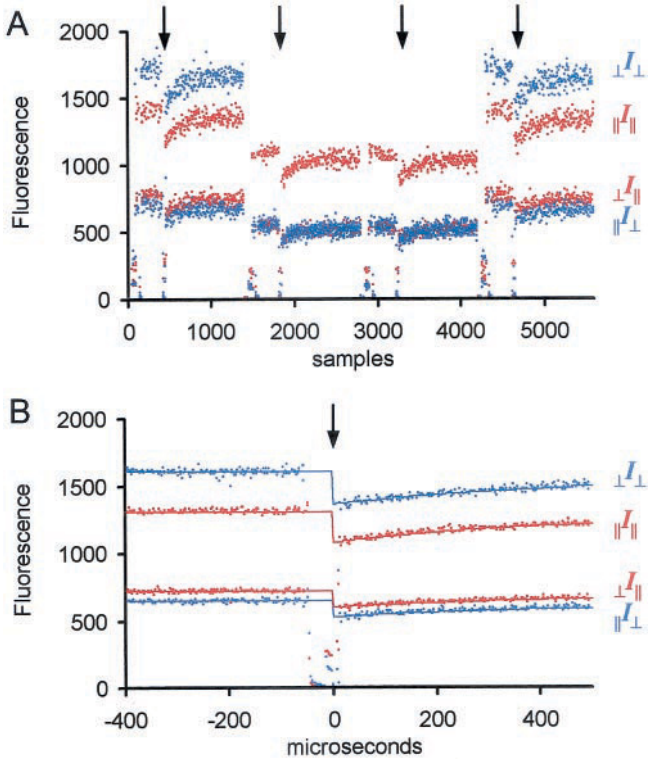

FIGURE 3 (*A*) Unprocessed fluorescence intensities representing parallel and perpendicularly polarized excitation and emission, as indicated on the right, from four PFD trials with illumination by the *x*, *y*, *y*, and *x* paths in succession. Bleach events are signified by *arrows*. The sample was a rigor muscle fiber as in Fig. 2. During *y*-illumination, ${}_{\perp}I_{\perp}$, ${}_{\perp}I_{\parallel}$, and ${}_{\parallel}I_{\perp}$ are superimposed, indicating that ${}^{y}Q_{\perp}$ is close to zero. (*B*) Averaged, uncorrected fluorescence intensity data from a complete sweep of 40 PFD trials, covering the period before and after the bleach events. *Smooth red and blue lines*: the average of steady pre-bleach fluorescence data, followed by a single exponential fitted to the post-bleach recoveries, corresponding to the four components of polarized fluorescence as indicated on the right.

2, lines representing the average of the constant fluorescence data before the bleach, and single exponential decays fitted to the recovery, are superimposed on the modulated PMT signals.

In order to gather polarized fluorescence data from both the parallel and perpendicular interrogation polarizations immediately after the bleach, each PFD trial was repeated with the excitation polarization switching 180° out of phase from that of the preceding trial (Fig. 2 *B*). Four individual trials with the input direction and polarization phase at (*x*, 0°), (*y*, 0°), (*y*, 180°), and (*x*, 180°) were completed as a set in that order (Fig. 3 *A*). Each complete sweep of the recording oscilloscope contained 10 such sets corresponding to 40 photoselection pulses and attendant recording of modulated polarized fluorescence. Recordings from each combination of input direction and polarization phase were averaged together later to improve signal-to-noise ratio. The duration of recording of the 10 sets was 17 seconds for muscle fiber data and 68 s for PVA reference samples. The reference samples were given longer dark times, appropriate to their longer triplet lifetimes.

Processing of fluorescence intensity data

Time-resolved intensity data

Data in each oscilloscope sweep were combined and corrected for instrumental imperfections as follows, using scripts written for MathCad PLUS 6.0e (MathSoft Corp, Cambridge, MA). For each direction of illumination, *x* and *y*, data from the consecutive trials at opposite phases of polarization switching were overlaid to obtain a complete time course for each excitation and emission polarization. Data recorded during the slewing time of the Pockels cell were set to zero and thereafter ignored. The ten repeats within an oscilloscope sweep of the 4-trial set of polarizations described above were overlaid and averaged to yield time-resolved, polarized fluorescence intensities, ${}^{x}_{\parallel}I^{u}_{\parallel}(t)$, ${}^{x}_{\perp}I^{u}_{\parallel}(t)$, ${}^{x}_{\parallel}I^{u}_{\perp}(t)$, ${}^{x}_{\perp}I^{u}_{\perp}(t)$, ${}^{y}_{\parallel}I^{u}_{\parallel}(t)$, ${}^{y}_{\perp}I^{u}_{\parallel}(t)$, ${}^{y}_{\parallel}I^{u}_{\perp}(t)$, and ${}^{y}_{\perp}I^{u}_{\perp}(t)$, uncorrected for the instrumental factors. Fig. 3, *A* and *B* show a partial set of these uncorrected time-resolved data on different time scales. Note that in Fig. 3 *A*, the time base is interrupted by dark intervals to allow triplet decay. The constant pre-bleach fluorescence intensities, ${}^{x}_{\parallel}I^{u}_{\parallel}$, ${}^{x}_{\perp}I^{u}_{\parallel}$, ${}^{x}_{\parallel}I^{u}_{\perp}$, ${}^{x}_{\perp}I^{u}_{\perp}$, ${}^{y}_{\parallel}I^{u}_{\parallel}$, ${}^{y}_{\perp}I^{u}_{\parallel}$, ${}^{y}_{\parallel}I^{u}_{\perp}$, and ${}^{y}_{\perp}I^{u}_{\perp}$, were obtained by averaging the uncorrected time-resolved intensity data over the 200 or 400 μs interval before the photoselection pulse.

Difference intensities

Time-resolved difference intensities, ${}^{x}_{\parallel}\Delta^{u}_{\parallel}(t)$, ${}^{x}_{\perp}\Delta^{u}_{\parallel}(t)$, ${}^{x}_{\parallel}\Delta^{u}_{\perp}(t)$, ${}^{x}_{\perp}\Delta^{u}_{\perp}(t)$, ${}^{y}_{\parallel}\Delta^{u}_{\perp}(t)$, ${}^{y}_{\perp}\Delta^{u}_{\parallel}(t)$, ${}^{y}_{\parallel}\Delta^{u}_{\perp}(t)$, and ${}^{y}_{\perp}\Delta^{u}_{\perp}(t)$, were obtained by subtracting each uncorrected time-resolved intensity from its corresponding steady-state intensity. To obtain a low-noise estimate of the difference intensities just after the photoselection pulse, a single exponential decay with offset was fitted to each time-resolved fluorescence intensity after the photoselection pulse and extrapolated back to time zero (the end of the photoselection pulse, Fig. 3 *B*). The fitting algorithm ignored data points taken within 20 μs of the photoselection pulse and during the Pockels cell slew between parallel and perpendicular polarizations. Data were fitted until approximately the $1/e$ time of triplet recovery. The back-extrapolated post-bleach fluorescence intensities were each subtracted from their corresponding pre-bleach values to yield time zero difference intensities, ${}^{x}_{\parallel}\Delta^{u}_{\parallel}$, ${}^{x}_{\perp}\Delta^{u}_{\parallel}$, ${}^{x}_{\parallel}\Delta^{u}_{\perp}$, ${}^{x}_{\perp}\Delta^{u}_{\perp}$, ${}^{y}_{\parallel}\Delta^{u}_{\parallel}$, ${}^{y}_{\perp}\Delta^{u}_{\parallel}$, ${}^{y}_{\parallel}\Delta^{u}_{\perp}$, and ${}^{y}_{\perp}\Delta^{u}_{\perp}$.

Instrumental correction factors

Differences between the interrogation and photoselection beam intensities among the various parallel and perpendicular polarizations and *x* and *y* directions, and differences between the detector sensitivities of the parallel and perpendicular PMTs, were measured using the calibration cube containing rhodamine in glycerol placed in the fiber position. For an isotropic sample, various fluorescence intensities are expected to be equal; ${}^{x}_{\perp}I_{\perp} = {}^{x}_{\parallel}I_{\parallel} = {}^{y}_{\parallel}I_{\parallel}$ and ${}^{y}_{\perp}I_{\perp} = {}^{x}_{\parallel}I_{\perp} = {}^{y}_{\parallel}I_{\perp} = {}^{x}_{\perp}I_{\parallel} = {}^{y}_{\perp}I_{\parallel}$, allowing determination of all of the relative interrogation beam intensities and detector sensitivities. Data from the rhodamine-glycerol cube and two rhodamine-PVA samples (isotropic and stretched), assayed at the beginning and end of each experiment, were averaged to obtain the instrumental correction factors that were applied to the experimental data.

Shifting of the fiber position after solution exchanges and mechanical drift sometimes caused slight trial-to-trial variation of PMT sensitivity and relative depth of bleaching between the *x* and *y* illumination. Corrections for these factors were recalculated for each trial using identities expected for a cylindrically symmetric sample containing probes with collinear absorption and emission dipoles: ${}^{x}_{\parallel}I_{\parallel} = {}^{y}_{\parallel}I_{\parallel}$, ${}^{x}_{\parallel}I_{\perp} = {}^{y}_{\parallel}I_{\perp} = {}^{x}_{\perp}I_{\parallel} = {}^{y}_{\perp}I_{\parallel}$, ${}^{x}_{\parallel}\Delta_{\parallel} = {}^{y}_{\parallel}\Delta_{\parallel}$, and ${}^{x}_{\parallel}\Delta_{\perp} = {}^{y}_{\parallel}\Delta_{\perp} = {}^{x}_{\perp}\Delta_{\parallel} = {}^{y}_{\perp}\Delta_{\parallel}$. Correction parameters derived from muscle fiber data differed from those determined on the random samples by no more than 2%. Instrumental correction coefficients were applied in appropriate combinations to the uncorrected intensities and differences to calculate 8 pre-bleach intensities, 8 zero-time difference intensities, and 8 time-resolved difference traces. Signals that are redundant on the basis of the cylindrical symmetry and collinearity of the absorption and emission dipoles were combined by averages, weighted by the inverse square of the standard deviations of each signal measured in each physiological condition, to produce the following 8 corrected signals: ${}_{\parallel}I_{\parallel}$, ${}_{\perp}I_{\parallel}$, ${}^{x}_{\perp}I_{\perp}$, ${}^{y}_{\perp}I_{\perp}$, ${}_{\parallel}\Delta_{\parallel}$, ${}_{\perp}\Delta_{\parallel}$, ${}^{x}_{\perp}\Delta_{\perp}$, and ${}^{y}_{\perp}\Delta_{\perp}$. For example, ${}_{\perp}I_{\parallel}$ represents the weighted average of

the corrected signals ${}^{x}_{\parallel}I_{\perp}$, ${}^{y}_{\parallel}I_{\perp}$, ${}^{x}_{\perp}I_{\parallel}$, and ${}^{y}_{\perp}I_{\parallel}$. These sets of intensities were normalized by I_0 and Δ_0 according to Eqs. D.27 and A.7 of the Appendix in order to combine them with data from other fibers. The triplet lifetime was determined by fitting a single exponential with offset to $I_0(t)$.

Analysis of fluorescence intensity and difference data

Calculation of polarization ratios and correlation functions

Normalized, polarized intensities for each biochemical condition were averaged in each experimental sample and polarization ratios were calculated from the final corrected intensities as:

$$Q_{\parallel} = \frac{{}_{\parallel}I_{\parallel} - {}_{\perp}I_{\parallel}}{{}_{\parallel}I_{\parallel} + {}_{\perp}I_{\parallel}}, \quad {}^{x}Q_{\perp} = \frac{{}^{x}_{\perp}I_{\perp} - {}_{\perp}I_{\parallel}}{{}^{x}_{\perp}I_{\perp} + {}_{\perp}I_{\parallel}}, \quad {}^{y}Q_{\perp} = \frac{{}^{y}_{\perp}I_{\perp} - {}_{\perp}I_{\parallel}}{{}^{y}_{\perp}I_{\perp} + {}_{\perp}I_{\parallel}},$$

Polarization ratios for the bleached population were calculated from the corrected time-resolved difference intensities as:

$$Q^{\Delta}_{\parallel}(t) = \frac{{}_{\parallel}\Delta_{\parallel}(t) - {}_{\perp}\Delta_{\parallel}(t)}{{}_{\parallel}\Delta_{\parallel}(t) + {}_{\perp}\Delta_{\parallel}(t)}, \quad {}^{x}Q^{\Delta}_{\perp}(t) = \frac{{}^{x}_{\perp}\Delta_{\perp}(t) - {}_{\perp}\Delta_{\parallel}(t)}{{}^{x}_{\perp}\Delta_{\perp}(t) + {}_{\perp}\Delta_{\parallel}(t)},$$

$${}^{y}Q^{\Delta}_{\perp}(t) = \frac{{}^{y}_{\perp}\Delta_{\perp}(t) - {}_{\perp}\Delta_{\parallel}(t)}{{}^{y}_{\perp}\Delta_{\perp}(t) + {}_{\perp}\Delta_{\parallel}(t)}.$$

To reduce noise, the time-resolved difference intensities were filtered with a low-pass 25-point, 2nd-order transversal filter (Savitsky and Golay, 1964) before calculation of these polarization ratios. The effective time resolution after filtering is 50 μs. Calculation of the $Q^{\Delta}(t)$ traces was terminated at 3 triplet decay times.

Order parameters were calculated from the pre-bleach correlation functions using Eqs. D.15–D.17 in the Appendix. Order parameters describing the microsecond-dynamic component were subsequently calculated by numerical fitting of δ_p, $\langle P_{2s}\rangle$, $\langle P_{4s}\rangle$ and $\langle P_{6s}\rangle$, to the data using Appendix Eqs. A.26–A.29.

RESULTS

Time-resolved intensities and polarization ratios

Reference samples

The polarized fluorescence depletion spectrometer was evaluated by testing three fluorescent samples with predictable behavior: IATR free to tumble in glycerol (Fig. 4), IATR immobilized in a polyvinyl alcohol (PVA) film but without any preferred orientation (Fig. 5 *A*), and IATR immobilized in a PVA film sample stretched to partially orient the fluorophores along the stretch axis (Fig. 5, *B–D*). Figs. 4 *A* and 5 *B* show time courses of fluorescence intensity, corrected for instrument imperfections as explained in Methods and averaged over 2 sweeps of 10 sets of photoselection/interrogation periods. The fluorescence intensity is plotted for 500 μs before the photoselection pulse, gated off during the photoselection (bleaching) period, and then plotted for 1 ms after the photoselection pulse. Of the four independent steady-state fluorescence intensities, ${}_{\parallel}I_{\parallel}$, ${}^{x}_{\perp}I_{\perp}$, ${}^{y}_{\perp}I_{\perp}$ and ${}_{\perp}I_{\parallel}$, two pairs are expected to be equal in isotropic samples, ${}_{\parallel}I_{\parallel} = {}^{x}_{\perp}I_{\perp}$ and ${}^{y}_{\perp}I_{\perp} = {}_{\perp}I_{\parallel}$.

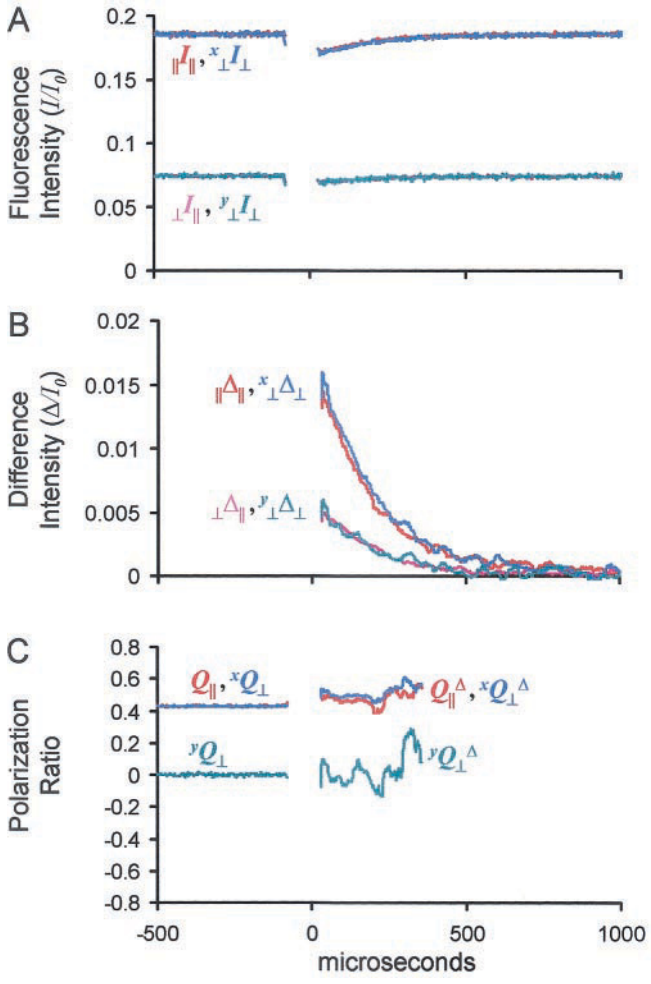

FIGURE 4 Fluorescence intensities (*A*), difference intensities (*B*), and polarization ratio data (*C*) from an IATR-glycerol reference sample. Time zero corresponds to cessation of the bleach pulse. Difference intensities (*B*) were obtained from fluorescence intensities before and after the photobleaching pulse as described in Materials and Methods. Polarization ratios (*C*) were calculated from fluorescence intensities before the bleach pulse, and from the difference intensities for 2–3 triplet lifetimes after the bleach pulse. The equalities ${}_{\parallel}I_{\parallel} = {}^{x}_{\perp}I_{\perp}$, ${}^{y}_{\perp}I_{\perp} = {}_{\perp}I_{\parallel}$, $Q_{\parallel}(t) \approx {}^{x}Q_{\perp}(t)$, and ${}^{y}Q_{\perp}(t) \approx 0$ arise from the isotropic probe orientation distribution. For this mobile sample, the analogous equalities ${}_{\parallel}\Delta_{\parallel}(t) = {}^{x}_{\perp}\Delta_{\perp}(t)$, ${}^{y}_{\perp}\Delta_{\perp}(t) = {}_{\perp}\Delta_{\parallel}(t)$, $Q^{\Delta}_{\parallel}(t) \approx {}^{x}Q^{\Delta}_{\perp}(t)$ and ${}^{y}Q^{\Delta}_{\perp}(t) \approx 0$ also apply after the bleach pulse. Polarization ratios arising from the bleached population ($Q^{\Delta}_{\parallel}$, ${}^{x}Q^{\Delta}_{\perp}$ and ${}^{y}Q^{\Delta}_{\perp}$) are similar to those before the bleach, indicating that the photobleached probes have returned essentially to the pre-bleach orientation distribution in the few microseconds between photoselection and interrogation.

These equalities are enforced for the IATR-glycerol sample (Fig. 4) in determination of the instrumental correction factors (Methods). The same equalities do not apply to the stretched PVA film of Fig. 5, *B–D* because of the order imposed by stretching that sample.

The fluorescence intensities measured after the photoselection pulse are briefly reduced, compared to those before the pulse, by depletion of the ground state due to population of the triplet state. The intensities return to their previous

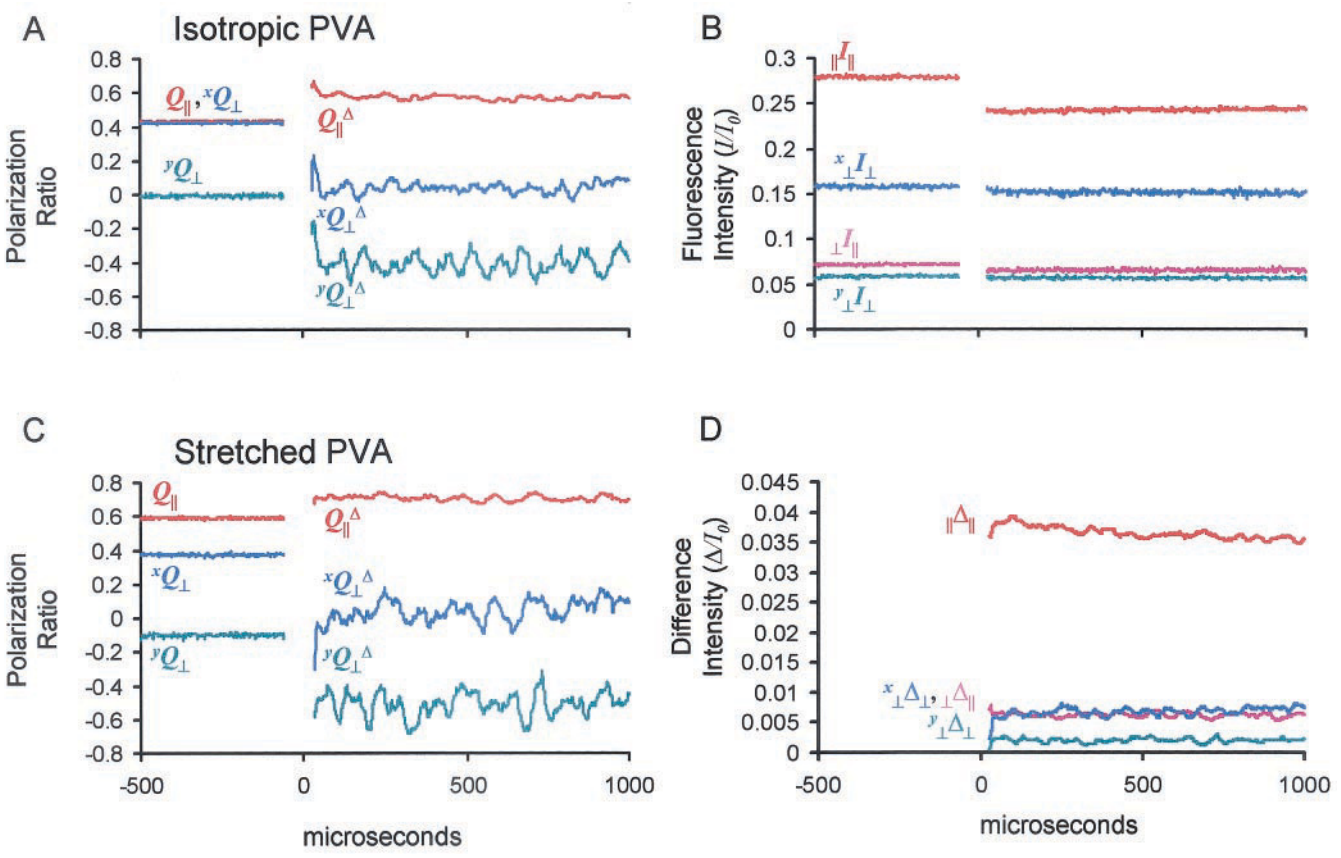

FIGURE 5 Fluorescence intensity, difference intensity, and polarization ratio data from isotropic and stretched IATR-PVA reference samples. (*A*) Polarization ratios for the unstretched PVA film. The sample is isotropic before the bleach pulse, but axially oriented afterwards. (*B*, *C*, *D*) Fluorescence intensities, polarization ratios and difference intensities, respectively, for a stretched PVA film. Before the bleach pulse, $_{\parallel}I_{\parallel} > {}^{x}_{\perp}I_{\perp}$, $^{y}_{\perp}I_{\perp} < {}_{\perp}I_{\parallel}$, $Q_{\parallel} > {}^{x}Q_{\perp}$, and $^{y}Q_{\perp} < 0$ indicating axial (parallel to the stretch axis) preference of the probe distribution. The time course of fluorescence recovery after photobleaching is slower than that of the glycerol sample (Fig. 4) because the film matrix inhibits quenching of excited triplets by molecular oxygen. After the bleach pulse, $_{\parallel}\Delta_{\parallel} \gg {}^{x}_{\perp}\Delta_{\perp}$, $^{y}_{\perp}\Delta_{\perp} < {}_{\perp}\Delta_{\parallel}$, $Q^{\Delta}_{\parallel} > Q_{\parallel}$, $^{x}Q^{\Delta}_{\perp} < {}^{x}Q_{\perp}$, and $^{y}Q^{\Delta}_{\perp} < {}^{y}Q_{\perp}$. These changes of the difference intensities and polarization ratio traces (e.g. $Q^{\Delta}_{\parallel}$ vs. $Q_{\parallel}$) at $t = 0$ indicate that the bleached population of probes is axially shifted relative to the pre-bleach distribution.

steady-state level by decay of the triplet population back to the ground state with a time constant ~200 μs in Fig. 4. During the triplet decay in Fig. 4, the fluorescence intensities obey the equalities $_{\parallel}I_{\parallel} = {}^{x}_{\perp}I_{\perp}$ and $^{y}_{\perp}I_{\perp} = {}_{\perp}I_{\parallel}$, indicating that the orientation of the unbleached population of fluorophores is isotropic. The bleached population is represented by the signals $_{\parallel}\Delta_{\parallel}(t)$, $^{x}_{\perp}\Delta_{\perp}(t)$, $^{y}_{\perp}\Delta_{\perp}(t)$ and $_{\perp}\Delta_{\parallel}(t)$ (Fig. 4B), obtained by subtracting the time course of the fluorescence recovery traces from the corresponding steady-state values. The bleached population is also isotropic as indicated by the observations that $_{\parallel}\Delta_{\parallel}(t) = {}^{x}_{\perp}\Delta_{\perp}(t)$ and $^{y}_{\perp}\Delta_{\perp}(t) = {}_{\perp}\Delta_{\parallel}(t)$. Polarization ratios calculated before the bleach pulse and also those representing the bleached population follow the behavior expected for isotropic samples: $Q_{\parallel}(t) \approx {}^{x}Q_{\perp}(t)$, $^{y}Q_{\perp}(t) \approx 0$, $Q^{\Delta}_{\parallel}(t) \approx {}^{x}Q^{\Delta}_{\perp}(t)$ and $^{y}Q^{\Delta}_{\perp}(t) \approx 0$ (Fig. 4 *C*, Table 1). Thus for rhodamine dissolved in glycerol, rotational diffusion is sufficiently fast that the anisotropy imposed on the bleached population by the photoselection event has decayed essentially to zero within the 20-μs interval

TABLE 1 Polarization ratios for the reference and muscle fiber samples

	$Q_{\parallel}$	$^{x}Q_{\perp}$	$^{y}Q_{\perp}$
Random glycerol	.397	.396	.001
S.E.M.	.0106	.0107	.0014
Random PVA film	.433	.433	−.008
S.E.M.	.0012	.00254	.0029
Axial stretched PVA	.589	.383	−.010
S.E.M.	.0010	.0025	.0022
Relaxed muscle	.277	.401	.062
S.E.M.	.0047	.0038	.0020
Rigor muscle	.116	.464	.110
S.E.M.	.0034	.0043	.0051
Active muscle	.274	.379	.039
S.E.M.	.0048	.0052	.0020

Polarization ratios were obtained from pre-bleach polarized fluorescence data as described in Materials and Methods. Each average value represents 6 muscle fibers, or measurements on the artificial samples on the same 6 days the fiber experiments were conducted. The artificial samples were measured before and after each muscle fiber experiment and the pre- and post-experiment values were averaged.

TABLE 2 Order parameters for the reference and muscle fiber samples

	$\langle P_{2d}\rangle$	$\langle P_2\rangle$	$\langle P_4\rangle$	$\delta_p(°)$	$\langle P_{2p}\rangle$	$\langle P_{4p}\rangle$	$\langle P_{2s}\rangle$	$\langle P_{4s}\rangle$	$\langle P_{6s}\rangle$
Random glycerol	.870	.0002	.002	92	−.001	.001			
S.E.M.	.014	.0003	.002	5	.043	.027			
Random PVA film	.927	.001	−.008	19	.91	.73	.001	−.012	−.064
S.E.M.	.003	.002	.002	2	.02	.05	.002	.003	.050
Stretched PVA	.960	.135	.049	25	.86	.59	.157	.088	−.025
S.E.M.	.002	.002	.002	2	.02	.06	.005	.011	.067
Relaxed muscle	.805	−.069	.004	56	.43	−.075	−.17	−.13	−.31
S.E.M.	.008	.001	.003	3	.04	.021	.02	.04	.38
Active muscle	.803	−.055	−.015	48	.56	.053	−.11	−.15	−.04
S.E.M.	.007	.001	.003	3	.05	.04	.02	.04	.26
Rigor muscle	.835	−.155	−.039	31	.79	.42	−.196	−.089	.004
S.E.M.	.005	.002	.006	1	.02	.03	.006	.008	.036

Order parameters were obtained from fluorescence and depletion data as described in Materials and Methods and the Appendix. $\langle P_{2d}\rangle$ reports restricted mobility of the dipoles on the sub-nanosecond time scale. $\langle P_2\rangle$ and $\langle P_4\rangle$ are order parameters of the probe distribution including the static orientation and microsecond motions. δ_p is the cone half-angle for the microsecond wobble used to generate the values for $\langle P_{2p}\rangle$ and $\langle P_{4p}\rangle$ according to the wobble-in-cone model. $\langle P_{2s}\rangle$, $\langle P_{4s}\rangle$ and $\langle P_{6s}\rangle$ are order parameters for the static orientation distribution with microsecond motions removed. For each of the samples, $n = 6$ as in Table 1.

between the photoselection pulse and measurement of the depleted fluorescence signals (the "dead time" of our instrument).

For the PVA films (Fig. 5), the triplet lifetime and recovery of fluorescence were extended relative to that of the glycerol sample, indicating that the film matrix stabilized the triplet excited state presumably due to its rigidity and/or reduced oxygen diffusion. The fluorescence signals recovered almost completely after a few hundred milliseconds.

For data from the unstretched rigid sample, $Q_\parallel = {}^xQ_\perp$ and ${}^yQ_\perp \approx 0$ before the photoselection pulse (Fig. 5 *A*, Table 1), indicating an isotropic probe distribution, but relative changes in intensities caused by the photoselection led to $Q_\parallel^\Delta > Q_\parallel$, ${}^xQ_\perp^\Delta < {}^xQ_\perp$, and ${}^yQ_\perp^\Delta < {}^yQ_\perp$. These inequalities indicate that the photobleaching pulse selects a population of probes with an orientation distribution that is preferentially in the parallel direction ($Q_\parallel^\Delta > {}^xQ_\perp^\Delta$, and ${}^yQ_\perp^\Delta < 0$), as expected from its parallel polarization. The three Q^Δ traces are stable on the timescale of Fig. 5 indicating that the parallel orientation of the bleached population is maintained due to the rigidity of the PVA film.

The stretched film (Fig. 5, *B–D*) has a preferential parallel orientation even before the photoselection pulse: $Q_\parallel > {}^xQ_\perp$, and ${}^yQ_\perp < 0$ (Fig. 5 *C*, Table 1), and the orientation distribution of the bleached population becomes more parallel: $Q_\parallel^\Delta > Q_\parallel$, ${}^xQ_\perp^\Delta < {}^xQ_\perp$, and ${}^yQ_\perp^\Delta < {}^yQ_\perp$ (Fig. 5C). These changes are stable on the timescale plotted in Fig. 5, but after several hundred milliseconds, the ground-state population returns to the pre-bleach distribution.

Order parameters obtained as described in the Appendix from fluorescence polarization and PFD data for a series of experiments on the reference samples are shown in Table 2. In all of the reference samples, the values of $\langle P_{2d}\rangle$ (0.87–0.96) indicate restricted mobility of the transition dipole moments on the sub-nanosecond time scale, equivalent to half-cone angles of 13°–24° in the standard random wobble-in-cone model (Kinosita et al., 1977). The near-zero values of $\langle P_2\rangle$ and $\langle P_4\rangle$ for the glycerol and unstretched PVA film describe an isotropic sample, and the positive values of $\langle P_2\rangle$ and $\langle P_4\rangle$ for the stretched PVA film indicate its axial ($\parallel$) preference.

For the glycerol sample, the half-cone angle, δ_p, for random wobble on the time scale 4 ns $\ll t \ll$ 20 μs (microsecond wobble, calculated from the steady-state and post-bleaching intensities as described in the Appendix) is close to 90°. The order parameters, $\langle P_{2p}\rangle$ and $\langle P_{4p}\rangle$ (Table 2), representing this motion are almost zero, indicating completely unrestricted rotational diffusion on the microsecond timescale, as expected for a liquid. The values of δ_p, $\langle P_{2p}\rangle$, and $\langle P_{4p}\rangle$ (Table 2), similar for the isotropic and stretched PVA films, show that the polymer restricts rotational mobility on the microsecond time scale.

The variables $\langle P_{2s}\rangle$, $\langle P_{4s}\rangle$ and $\langle P_{6s}\rangle$ are the order parameters for the static probe distribution after allowing for the effects of both sub-nanosecond ($\langle P_{2d}\rangle$) and microsecond ($\langle P_{2p}\rangle$ and $\langle P_{4p}\rangle$) motions. These are all nearly zero for the isotropic PVA sample and, except for $\langle P_{6s}\rangle$, significantly different from zero for the stretched film. In the case of the glycerol sample, the values of $\langle P_{2p}\rangle$ and $\langle P_{4p}\rangle$ being indistinguishable from zero prevented meaningful determination of $\langle P_{2s}\rangle$, $\langle P_{4s}\rangle$, or $\langle P_{6s}\rangle$, but those parameters are also expected to be zero.

A simple model for the orientation distribution of the probes in the PVA films assumes that the probe molecules are aligned either parallel or perpendicular to the polymer strands in the film. In the unstretched film, the polymer strands are oriented equally at all angles, so the probe orientation distribution is isotropic and $\langle P_{2s}\rangle$, $\langle P_{4s}\rangle$ and $\langle P_{6s}\rangle$ are all zero. If the polymer strands reorient to accommodate

the stretch without changing the volume of the film, then the strand orientation probability distribution is given by

$$h(\beta) = \frac{1}{2}\frac{S^2}{[1 + (S^2 - 1)\sin^2 \beta]^{3/2}} \quad (4)$$

where S is the length:width ratio of the stretched film relative to its original dimensions (Michl and Thulstrup, 1986). The 2nd rank order parameter for the strands, $\langle P_{2str}\rangle$, is given (cf. Eq. 2 of Dale et al., 1999), by:

$$\langle P_{2str}\rangle = \int_0^{\pi} P_2(\cos\beta)h(\beta)\sin\beta\, d\beta$$

while for the component of probes perpendicular to the strands, $\langle P_{2per}\rangle$, an additional integration around the azimuth (ϕ) of each strand is required:

$$\langle P_{2per}\rangle = \frac{1}{\pi}\int_0^{\pi}\int_0^{\pi} P_2(\sin(\beta)\cos(\phi))h(\beta)\sin(\beta)d\beta\, d\phi.$$

The 2nd-rank order parameter for the probes is then given by:

$$\langle P_{2s}\rangle = \alpha\langle P_{2str}\rangle + (1 - \alpha)\langle P_{2per}\rangle \quad (5)$$

where α is the fraction of probe molecules aligned with the PVA strands and $(1 - \alpha)$ is the fraction of probes aligned perpendicular to the strands. $\langle P_{4s}\rangle$ and $\langle P_{6s}\rangle$ are calculated similarly. Values of the order parameters for this simple model of the stretched film at values of $S = 2.1$ and $\alpha = 0.67$ are $\langle P_{2s}\rangle = 0.159$, $\langle P_{4s}\rangle = 0.087$ and $\langle P_{6s}\rangle = 0.022$, quite close to those observed (Table 2, stretched film). Although the film was stretched approximately 5-fold, the lower apparent value of S probably indicates annealing and rearrangement of the polymer strands at the high temperature applied during the stretch. Nevertheless, the experiments on the reference samples show that the PFD signals readily distinguish relatively rigid samples (both PVA films) from the mobile one (the glycerol sample) and that, in sufficiently rigid samples, an extra order parameter of the static orientation distribution ($\langle P_{6s}\rangle$) can be estimated.

Muscle fiber data

Fig. 6 shows time courses of fluorescence intensity, fluorescence depletion (difference intensities), and polarization ratios from a relaxed muscle fiber. In all three physiological states, relaxed, contracting and rigor, the steady-state probe orientation distribution had perpendicular preference as indicated by ${}^{x}Q_{\perp} > Q_{\parallel}$ and ${}^{y}Q_{\perp} > 0$ (Table 1). The probes are most perpendicular in rigor (${}^{x}Q_{\perp} \gg Q_{\parallel}$, Fig. 7A), as reported previously (Allen et al., 1996, Hopkins et al., 1998).

Transiently decreased fluorescence intensity after zero time (Fig. 6A) indicates photoselection of a population of

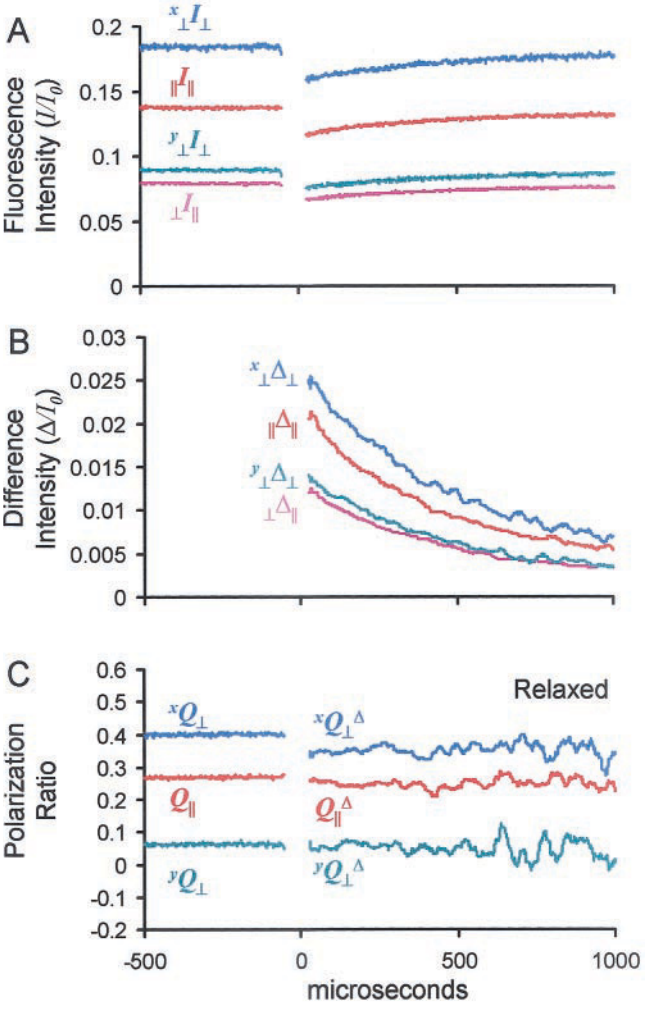

FIGURE 6 Fluorescence intensities (*A*), difference intensities (*B*), and polarization ratio data (*C*) from a muscle fiber in the relaxed state. Note that the ratios ${}^{x}_{\perp}I_{\perp} : {}_{\parallel}I_{\parallel} : {}^{y}_{\perp}I_{\perp} : {}_{\perp}I_{\parallel}$ are similar to the ratios ${}^{x}_{\perp}\Delta_{\perp} : {}_{\parallel}\Delta_{\parallel} : {}^{y}_{\perp}\Delta_{\perp} : {}_{\perp}\Delta_{\parallel}$. Thus, the polarization ratios arising from the bleached population (Q^{Δ}) are similar to those of the entire sample before fluorescence depletion (except for some deflection of ${}^{x}Q^{\Delta}_{\perp}$ compared to ${}^{x}Q_{\perp}$), suggesting that the sample has reoriented extensively in the time between photoselection and interrogation.

probes by the bleaching pulse. When a single exponential decay toward the pre-bleach fluorescence was fitted to the total fluorescence ($I_0 = {}_{\parallel}I_{\parallel} + 4\,{}_{\perp}I_{\parallel} + 2\,{}^{x}_{\perp}I_{\perp} + 2\,{}^{y}_{\perp}I_{\perp}$), the time constant, τ_t, corresponding to the triplet-state lifetime, was 450 ± 7 μs (S.E.M., $n = 6$) in the relaxed state, 460 ± 15 μs in the rigor state, and 540 ± 18 μs in the isometric contracting (active) state. τ_t was significantly greater in the active state than in relaxation or rigor. This difference might be due to an altered probe environment in the active state, even though the sub-nanosecond mobility ($\langle P_{2d}\rangle$) is equal to that in relaxation. Alternatively, active contractions in this work were kept very brief, perhaps allowing the oxygen scavenging system to maintain a lower oxygen tension in

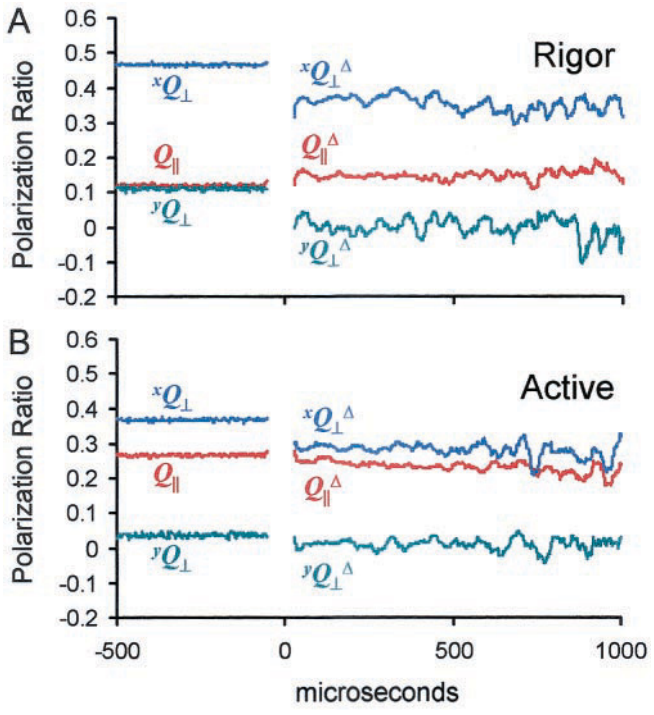

FIGURE 7 Polarization ratios from muscle fiber samples in the rigor (*A*) and active (*B*) states. The changes of the polarization ratio traces after the photobleaching pulse relative to those before it (e.g., ${}^{x}Q_{\perp}^{\Delta} < {}^{x}Q_{\perp}$) indicate that the bleached population of probes is shifted axially relative to the pre-bleach distribution, especially in the rigor case (*A*).

that condition, leading to decreased quenching of probe triplet states.

Selection of a parallel population by the photobleaching pulse is seen in the muscle fiber recordings by shifts in the polarization ratios after each bleaching pulse. For all three physiological states, ${}^{x}Q_{\perp}^{\Delta} < {}^{x}Q_{\perp}$ and ${}^{y}Q_{\perp}^{\Delta} < {}^{y}Q_{\perp}$. These differences are most pronounced in rigor (Fig. 7 *A*), smallest in relaxation (Fig. 6 *C*). In rigor, $Q_{\parallel}^{\Delta}$ for the bleached population was greater than $Q_{\parallel}$, also indicating a strongly parallel photoselected population. In relaxation and active contraction, $Q_{\parallel}^{\Delta}$ was either the same or slightly less than $Q_{\parallel}$, suggesting that, within the 20 μs dead time before measuring $Q_{\parallel}^{\Delta}$, the orientation of the photoselected population had decayed from the more parallel preference imposed by the bleaching pulse back towards that of the unselected population.

The order parameters calculated from the muscle fiber fluorescence polarization and PFD data (Table 2) show similar values of $\langle P_{2d}\rangle$ in relaxation and contraction, indicating that the extent of restricted sub-nanosecond probe mobility is similar. $\langle P_{2d}\rangle$ is slightly higher in rigor than in the other two states as reported before (Hopkins et al., 1998; Dale et al., 1999), indicating that in rigor the fast probe motions are slightly more restricted. The values of $\langle P_2\rangle$ are all negative indicating that the "average" probe orientations relative to the fiber axis are >54.7°. On the other hand δ_p, $\langle P_{2p}\rangle$ and $\langle P_{4p}\rangle$, giving the extent of microsecond motions, are very different between the relaxed, contracting and rigor conditions. Relaxed muscle fibers have the least restricted motions (largest δ_p, smallest $\langle P_{2p}\rangle$ and $\langle P_{4p}\rangle$), rigor the most restricted (smallest δ_p, and highest $\langle P_{2p}\rangle$ and $\langle P_{4p}\rangle$). Activation was intermediate.

$\langle P_{2s}\rangle$ and $\langle P_{4s}\rangle$, the order parameters for the static distribution after "factoring out" the microsecond motion, all have larger negative values than $\langle P_2\rangle$ and $\langle P_4\rangle$, due to removal of the depolarizing effect of the microsecond motions. The magnitude of $\langle P_{2s}\rangle$ was largest in rigor indicating the most perpendicular distribution. $\langle P_{2s}\rangle$ and $\langle P_{4s}\rangle$ in activating solution do not lie between the relaxed and rigor values, indicating that the orientation distribution in active muscle is not a combination of components with the distributions of relaxed and rigor muscle fibers. The value of $\langle P_{6s}\rangle$ in rigor is close to zero suggesting that the static orientation distribution does not have major sharp features beyond those described by $\langle P_{2s}\rangle$ and $\langle P_{4s}\rangle$. Values obtained for $\langle P_{6s}\rangle$ in relaxation and activation are not reliable because extensive microsecond motions lead to small values of $\langle P_{2p}\rangle$ and $\langle P_{4p}\rangle$, and to excessive variability from fiber to fiber of $\langle P_{6s}\rangle$.

All of the fluorescence difference intensity (Δ) traces from the muscle fibers were very close to single exponential decays with triplet lifetime τ_t, leading to essentially constant polarization signals ($Q_{\parallel}^{\Delta}(t)$, ${}^{x}Q_{\perp}^{\Delta}(t)$, and ${}^{y}Q_{\perp}^{\Delta}(t)$ for the bleached population. This result indicates that the motions that depolarize the photoselected population are virtually complete within the 20 μs dead time. Some individual muscle fibers displayed deflections in their $Q^{\Delta}(t)$ traces, but these were not reproducible. As the kinetics of tilting motions during isometric contraction detected following mechanical perturbations are somewhat slower than this time scale (e.g., Irving et al., 1995), we tested whether a small deflection of the $Q^{\Delta}(t)$ signals would be resolved in the active state if the random noise was diminished by averaging data from several muscle fiber experiments (Fig. 8). No appreciable deflections of the $Q^{\Delta}(t)$ signals were detected in the averaged traces (*panel C*), confirming that the motions of the photoselected population reach a restricted angular distribution within the 20 μs instrumental dead time and maintain that distribution for at least a few milliseconds.

Intensity of the interrogation beam

In the PFD method, the intensity of the steady-state fluorescence excitation beam has to be adjusted to obtain usable signal-to-noise ratio while minimizing steady-state population of the triplet state. In Fig. 9, a sample of rhodamine-labeled BSA in rigor solution was illuminated with increasing intensity during the interrogation phase of the PFD experiment. The flat (*blue*) traces show trials with no photoselection pulse. At very low intensity (*panel A*), the fluorescence signals are noisy mainly due to Poisson statistics

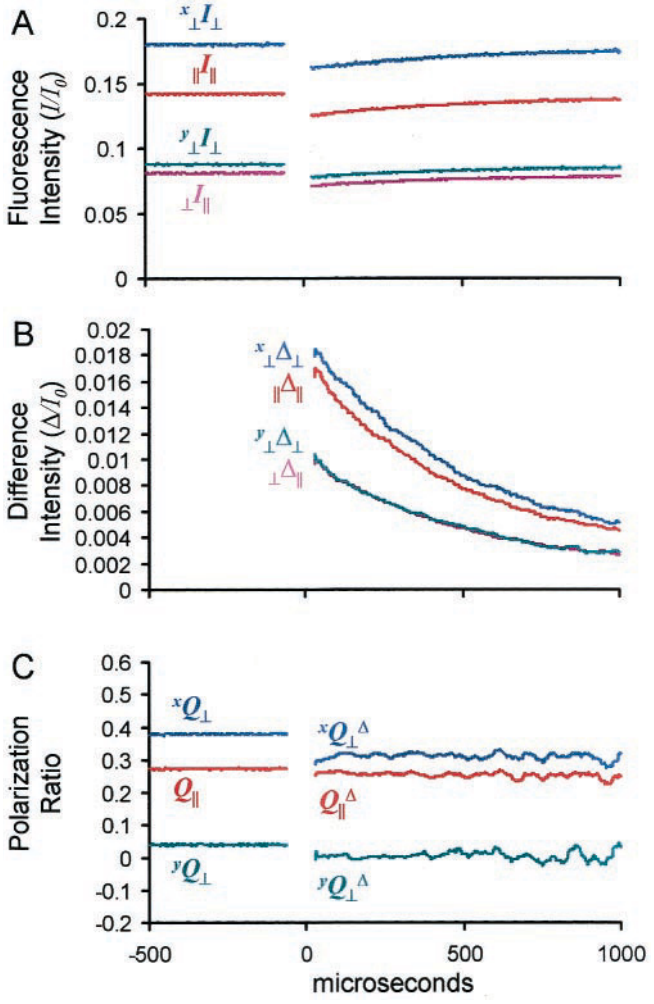

FIGURE 8 Averaged fluorescence intensities (*A*), difference intensities (*B*), and polarization ratio data (*C*) from six muscle fiber samples in the active, isometrically contracting state. The polarization ratio traces are similar to those in Fig. 7 *B*, but less noisy. There are no reproducible deflections of the Q^{Δ} traces after ~100 μs following the bleaching pulse at time zero, indicating that motions of the active cross-bridges are fast.

of the number of detected photons. As the intensity of the excitation increased, the fluorescence intensity relative to the noise increased (*panels B–D*). However, the amount of transient photobleaching relative to the steady fluorescence decreased at high intensities. This decrease is due to partial steady-state population of the triplet state by the interrogation beam and consequent diminution of the ground state (Johnson and Garland, 1981, 1982). The smaller relative bleaching increases the uncertainty of estimating the extent of depletion. Population of the triplet state by pumping with the interrogation beam may also perturb the probe orientation distribution (Axelrod et al., 1976; Hellen and Burghardt, 1994). These factors are disadvantages of using an intense interrogation beam. The decay of fluorescence depletion also becomes faster at high interrogation intensities (Fig. 9 *D*). The observed decay rate is equal to the sum of the rate of triplet formation (pumping rate) and rate of triplet decay. When these two rates begin to become comparable at high interrogation intensity, the observed rate increases.

These parameters, plotted against the intensity of fluorescence emission during the interrogation period (Fig. 10), show that an intermediate range of steady-state excitation provides the optimum overall signal-to-noise ratio (*panel D*). Muscle fiber experiments were conducted in the range where the signal-to-noise ratio was rising with interrogation intensity and the observed rate of decay of fluorescence depletion was constant.

Intensity of the photoselection pulse

As described in the Theory section, excessive transient photobleaching can lead to a distribution of the bleached population that is altered (flattened) from the ideal $\cos^2\theta$ function. To determine the appropriate range of photoselection pulses and the effect of this expected flattening, PFD experiments were conducted over a range of bleach pulse intensities. Correlation functions of the bleached population (Eqs. A.11–A.13 in the Appendix) were measured at a range of bleach depths (Fig. 11). Curvilinear relations (Eqs. A.30–A.32) fitted to the observed correlation parameters yield values that may be extrapolated to infinitesimal bleach for these parameters. In these experiments, δ_p, the cone half-angle for the microsecond wobble, estimated by this procedure was reduced by approximately 3° in rigor and 20° in relaxed fibers. These differences do not alter the conclusions derived from the experiments at moderate bleach levels, but they do indicate that the depth of photobleaching in a PFD experiment should be chosen carefully.

DISCUSSION

Following a brief intense pulse of light, the fluorescence from rhodamine probes bound to myosin RLC in muscle fibers and excited by a weak continuous beam was transiently diminished due to population of the triplet excited state and consequent diminution of the ground state. The orientation distribution of the remaining unbleached probes provided information about mobility on the time scale between 20 ns and 20 μs. As expected, the mobility in relaxed muscle is higher than that in rigor and intermediate during active contraction (Table 2, $\langle P_{2p}\rangle$ and $\langle P_{4p}\rangle$). Faster ($\ll$1 ns) motions of the probes relative to the attached protein, are very similar in the three physiological states suggesting that the mobility on the intermediate (20 ns $< t <$ 20 μs) time scale reflects rotational motions of the RLC. The latter motions probably represent thermally driven random reorientation over a restricted angular range and/or biochemically driven tilting related to force generation.

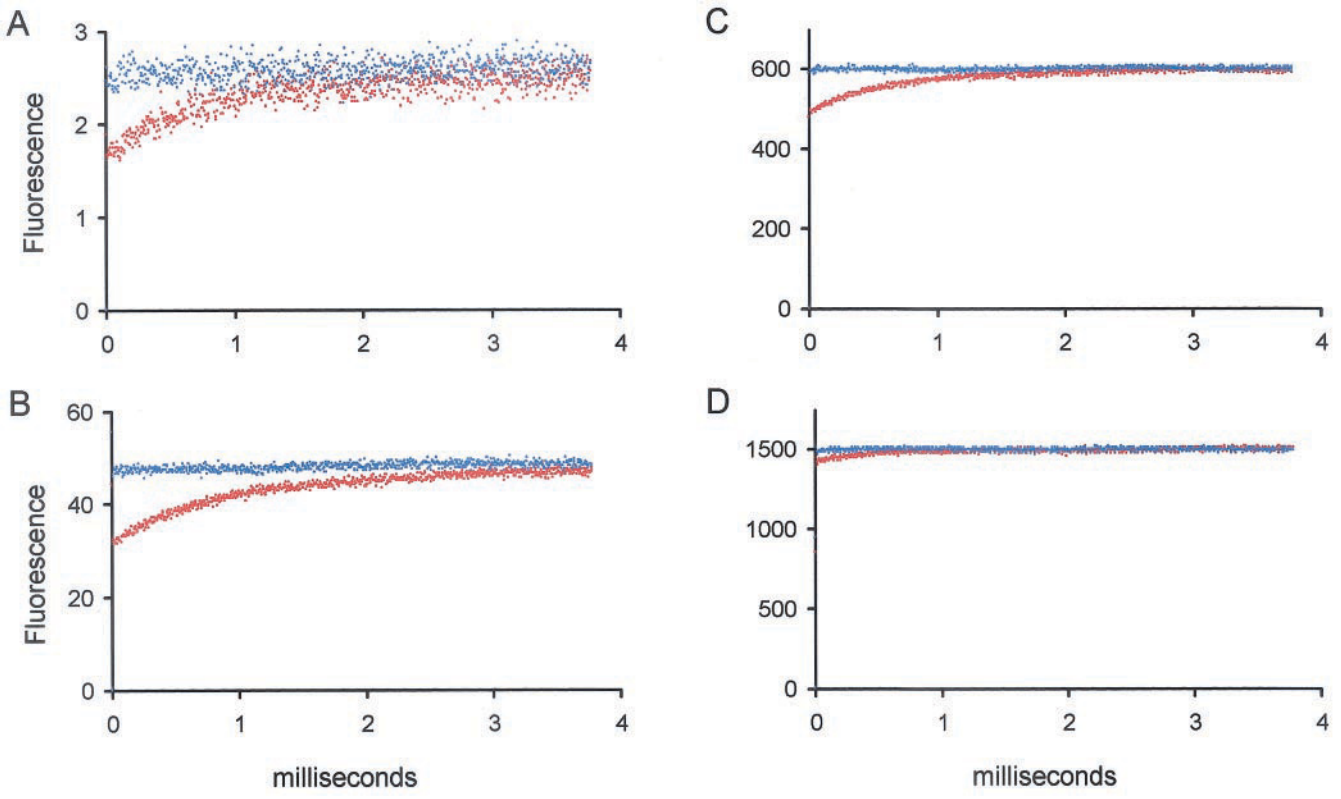

FIGURE 9 Representative data from an experiment to determine depletion as a function of increasing emission intensity, using the IATR-labeled BSA. For each bleach trial (*red traces*), a null trial (*blue traces*) was performed without the high intensity photoselection. The blue traces are flat, showing that any artifacts due to recovery from electronic gating are small compared to the reduction of fluorescence after the photobleaching pulse on the time-scale monitored. Excitation intensity and consequent emission are increased from panels *A* through *D*. The signal-to-noise ratio increases with excitation intensity. At very high excitation intensities, both the relative amplitude of fluorescence depletion and the lifetime of the triplet state (the time constant of the fluorescence recovery) decrease (see also Fig. 10 *A*).

The orientation distribution of the RLC is also broader during active contraction than in rigor. Whether or not this additional dispersion of orientations rests in the same process that contributes to the mobility can be tested by calculating the static orientation distribution after removing the effect of the motions on both fast and intermediate time scales. The calculation is presented below, and shows that most of the increased breadth of the RLC distribution in active contraction is due to the rotational motions on the time scale of 20 ns to 20 μs.

Surprisingly, all of the motions were completed within the ~20 μs dead time of our instrumentation, and we did not directly observe the time course of the microsecond reorientation. The altered angular distribution 20 μs after the bleaching pulse, when interrogation was resumed, is then interpreted as restriction of the amplitude of reorientation completed within 20 μs. Direct detection of the time course of this motion would require a briefer transient photobleaching pulse than obtained with the modulated continuous-wave laser used in the present study. Nevertheless, both the restricted rotational motion and the static order could be inferred from our data and quantified.

Polarized fluorescence bleaching method

Johnson and Garland (1981, 1982) and Barisas and colleagues (Yoshida and Barisas, 1986; Yoshida et al., 1988; Rahman et al., 1992) introduced transient polarized photobleaching as a sensitive method for detection of protein rotational motions on the μs − ms time scale. We have extended the theoretical basis for analyzing PFD experimental data to systems with inherent order. Along with the present application in muscle fibers, the analysis should be applicable to experiments on other ordered systems such as oriented membranes.

Three separate polarized optical photoselection events are involved in measuring PFD: transient excitation of an appreciable portion of the probes into the triplet state, low-level excitation of the remaining ground state (singlet) molecules by a weak interrogation beam, and detection of fluorescence from the excited singlet population. Fluorescence polarization measurements usually involve only the latter two events. Due to the extra photoselection, PFD is capable of providing enhanced resolution of the probe angular distribution (for low fractions of triplet population up

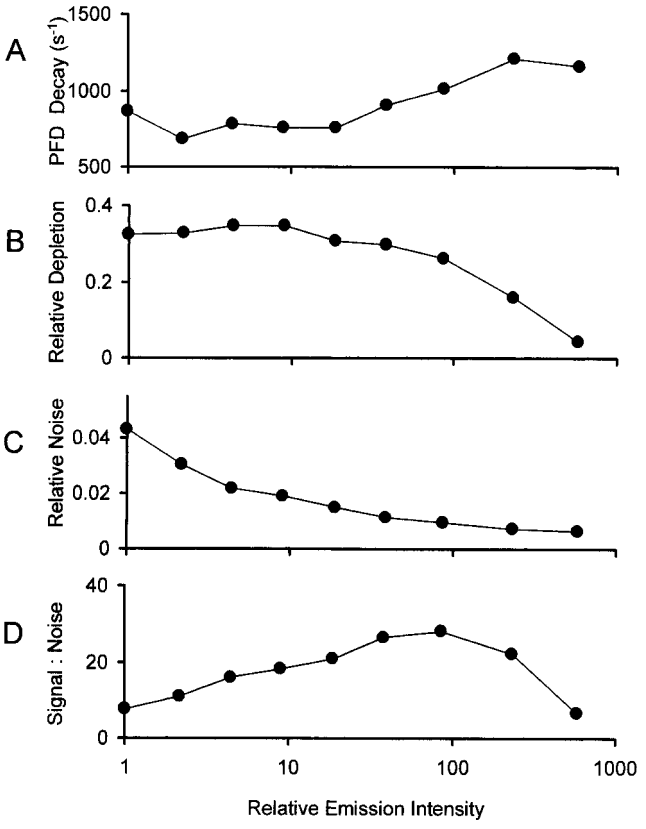

FIGURE 10 Analysis of fluorescence depletion as a function of emission intensity. The sample is IATR-labeled BSA as in Fig. 9. Single exponential functions were fitted to the post-bleach fluorescence recovery in Fig. 9. (*A* and *B*) Rate constant and relative amplitude of the fitted exponential functions are plotted *vs*. relative fluorescence intensity. (*C*) The noise (standard deviation during a 1 ms window) in the fluorescence signal. (*D*) The ratio of exponential amplitude (from *B*) to relative noise (*C*). The signal-to-noise ratio is greatest at an intermediate excitation intensity.

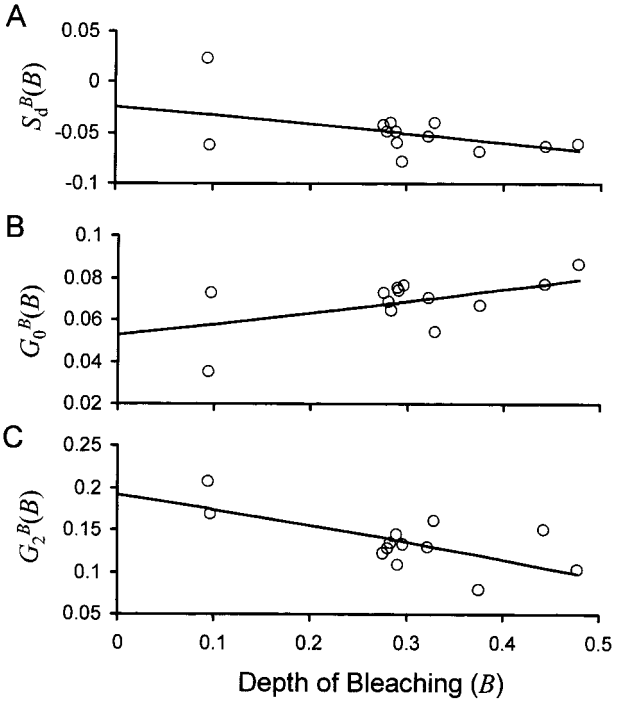

FIGURE 11 Bleach-dependent correlation functions obtained over a range of bleach depths. The *open circles* are the values of the correlation functions (Eqs. A.11–A.13 in the Appendix) calculated from the intensity data. The *solid lines* are the results of fitting Eqs. A.30–A.32 to the data. Extrapolation of the fitted lines to zero bleach depth (left-hand ordinate) gives estimates of the correlation functions at zero bleach depth.

to the 6th-rank order parameter, $\langle P_{6s}\rangle$, of the static probe angular distribution containing terms in $\cos^6\beta$, where β is the probe angle relative to the symmetry axis of the sample). The broadening effect of probe motions on the intermediate time scale of 20 ns $< t <$ 20 μs are "factored out" from the static distribution described by $\langle P_{2s}\rangle$, $\langle P_{4s}\rangle$ and $\langle P_{6s}\rangle$. Conventional fluorescence polarization measurements provide order parameters combining the static distribution and motions on the intermediate time scale, and are limited to order parameters up to the 4th rank. Theoretically, at higher bleach intensities, higher order information ($\langle P_{8s}\rangle$, etc.) is obtainable using PFD. In practice, even the $\cos^6\beta$ information from muscle fibers is rather noisy, limiting its usefulness, but the parameters expressing the extent of motion on the intermediate time range and the static order parameters up to the 4th rank are reliable.

The experimental setup and analysis were evaluated using artificial samples with predictable orientation distributions and probe mobilities. The PFD instrument correctly distinguished among the isotropic highly mobile glycerol sample, the very much less mobile, but still isotropic, PVA film, and the ordered stretched PVA film. The order parameters defining extent of reorientational mobility and static orientation distribution measured using the PFD technique on these calibration samples (Table 2) were in reasonable agreement with values expected for these artificial samples, indicating the reliability of the instrumentation and analysis. In addition, symmetries in the calibration samples enabled correction of instrumental imperfections, such as differences in illumination intensities and detector sensitivities. Determinations of some these instrumental factors based on the cylindrical symmetry of the muscle fibers gave very similar values, indicating that the corrected intensities do indeed reflect the probe orientation distributions and mobilities.

Maximum entropy distributions

The measured order parameters, $\langle P_2\rangle$, $\langle P_4\rangle$, etc., carry angular information because they are coefficients of the first few terms of a series expansion that describes the probe orientation distribution (e.g., Dale et al., 1999). However, many more order parameters than available from fluorescence experiments would need to be determined to directly

calculate a realistic orientation distribution using the series expansion. A useful method to estimate the distribution with the limited information provided by a few order parameters is the maximum entropy (ME) distribution (van der Heide et al., 2000). The ME distribution is the broadest orientational distribution consistent with the observed order parameters. For the first two even-rank order parameters, it is given by

$$f_{ME}(\beta_{fp}) = \exp\{-\lambda_0 - \lambda_2 P_2(\cos\beta_{fp}) - \lambda_4 P_4(\cos\beta_{fp})\} \quad (6)$$

where $f_{ME}(\beta_{fp})$ is the distribution with respect to the angle, β_{fp}, between the probe and the fiber axis, and $P_2(z) = (3z^2 - 1)/2$, $P_4(z) = (35z^4 - 30z^2 + 3)/8$. The coefficients λ_0, λ_2 and λ_4, termed Lagrange multipliers, are adjusted by a numerical algorithm until the 2nd and 4th-rank order parameters (averages of the functions $P_2(\cos\beta_{fp})$ and $P_4(\cos\beta_{fp})$ over the ME distribution) are equal to the measured ones,

$$\langle P_2\rangle = \int_0^{\pi} P_2(\cos\beta_{fp}) f_{ME}(\beta_{fp}) \sin\beta_{fp}\, d\beta_{fp}$$

and

$$\langle P_4\rangle = \int_0^{\pi} P_4(\cos\beta_{fp}) f_{ME}(\beta_{fp}) \sin\beta_{fp}\, d\beta_{fp}$$

and $f_{ME}(\beta_{fp})$ is normalized so that $\int_0^{\pi} f_{ME}(\beta_{fp})\sin\beta_{fp} d\beta_{fp} = 1$.

Fig. 12 *A* shows the static ME distribution for the active contracting state (*blue curve*). The order parameters used are $\langle P_{2s}\rangle$ and $\langle P_{4s}\rangle$ (Table 2), representing the static distribution after "factoring out" the effect of the rapid ($\langle P_{2d}\rangle$) and intermediate ($\langle P_{2p}\rangle$ and $\langle P_{4p}\rangle$) time scale motions (Eq. 3 in the Theory section). The ME distribution has a peak at 58° and another peak at 180° − 58° = 122° due to the dipole nature of the probes and the twofold symmetry of the sarcomere. All distributions determined using only even-rank order parameters are symmetrical around $\beta = 90°$. This ME distribution is a unique and equivalent representation of the fluorescence polarization data. However, the real distribution of the probe within one half of the sarcomere is probably mainly situated above or below 90°. If we approximate the distribution of the probes as a single, roughly symmetrical peak either above or below 90°, then the two lowest odd-rank terms can be added to the equation for the ME distribution:

$$f_{MEO}(\beta_{fp}) = \exp\{-\lambda_0 - \lambda_1 P_1(\cos\beta_{fp}) - \lambda_2 P_2(\cos\beta_{fp}) - \lambda_3 P_3(\cos\beta_{fp}) - \lambda_4 P_4(\cos\beta_{fp})\} \quad (7)$$

where $P_1(z) = z$ and $P_3(z) = (5z^3 - z)/2$. The Lagrange multipliers λ_1 and λ_3 are obtained by noting that the value

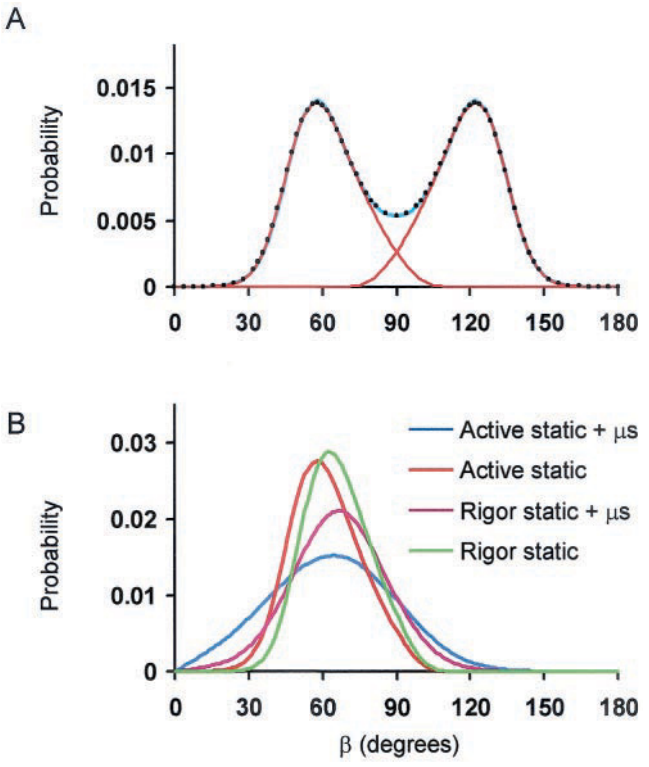

FIGURE 12 Maximum entropy distributions of the probe angle, β, relative to the muscle fiber axis. (*A*) Static orientation distribution (*blue curve*) during active contraction based on $\langle P_{2s}\rangle$ and $\langle P_{4s}\rangle$ in Table 2. The corresponding Lagrange coefficients defining the distribution in Eq. 6 are $\{\lambda_0, \lambda_2, \lambda_4\} = \{1.08, 1.78, 2.65\}$. The *red curves* are one-sided ME distributions (Eq. 7) generated as described in the Discussion, on the assumption that each distribution reaches zero at the opposite peak of the two-sided distribution. The red curves are scaled such that the total probability given by each is 0.5. The distribution represented by *black dots* is the sum of the two red curves and closely overlays the original (*blue*) two-sided distribution. (*B*) One-sided ME distributions for active contraction including microsecond motions (*blue*), active excluding microsecond motions (*red*), rigor including microsecond motions (*magenta*), and rigor excluding microsecond motions (*green*). All plotted distributions are probabilities given by Eq. 6 or 7 multiplied by sin β.

of the original two-peaked ME distribution ($f_{ME}(\beta_{fp})$) and an equivalent normalized one-sided distribution ($f_{MEO}(\beta_{fp})$) are the same at $\beta_{fp} = 90°$ and assuming either that the distribution is symmetrical (i.e., the centroid of $f_{MEO}(\beta_{fp})\sin\beta_{fp}$ is at the same angle as its peak) or that the one-sided distribution is zero at the peak of its reflection across the 90° plane (at 180° − 58° in Fig. 12 *A*). The latter one-sided ME distribution and its image (180° − β_{fp}) are shown as red curves in Fig. 12 *A*. Their peaks and widths are well defined by the original two-sided distribution. The sum of the two one-sided ME distributions (*black dots*) is very similar to the original two-sided ME distribution. We will present one-sided ME distributions in the remainder of this Discussion because they represent the likely distribution for a half sarcomere. It should be noted, however, that the two-sided distribution is a more direct representation of the data be-

cause of the extra assumption used to generate the single-peaked curve.

Cross-bridge orientation and motions

The one-sided ME orientation distribution calculated from $\langle P_2 \rangle$ and $\langle P_4 \rangle$ (Table 2) for active muscle (Fig. 12 *B*, *blue curve*) peaks at 64° and has a full width at half maximum (FWHM) of 63°. The corresponding values for the rigor distribution are peak 67° and FWHM 42° (*magenta curve*). When the intermediate time scale ($\ll$20 μs) motions are factored out, the resultant static distributions are narrower. The FWHM in active contraction and rigor are 34° (*red curve*) and 33° (*green curve*) respectively, much closer to each other than in the distributions including the motions. Thus the increased dispersion of orientation in active contraction compared to rigor is accounted for by the intermediate time scale motions. The same conclusion follows from the decrease in width (δ_p) of the wobble cone for the intermediate time scale, 48° in activation and 31° in rigor (Table 2).

The static rigor distribution peaks at 63°, whereas the active one peaks at 58°, indicating that the probes on the RLC are oriented more perpendicular to the fiber axis than in activation. The difference (5°) is small, probably because a relatively small proportion of the cross-bridges contribute to generation of active tension (Hopkins et al., 1998, 2002; Corrie et al., 1999).

Compared to those in activating and rigor conditions, the orientation distribution for relaxing solution is wider, enough so that two peaks on either side of 90° are not resolved (not shown). The increased width is consistent with the greater range of intermediate time scale motion (δ_p = 56°), indicating that the orientation distribution including this motion is spread over the entire 0°–180° angular range. Thus the PFD method indicates highly mobile myosin heads in relaxed muscle. The values of $\langle P_{2p} \rangle$ and $\langle P_{4p} \rangle$ (for the intermediate time scale motion) are consequently smallest in relaxation. The range of probe motion on the time scale faster than the fluorescence lifetime is also slightly broader in relaxation and activation than in rigor, as indicated by their slightly decreased $\langle P_{2d} \rangle$ values, as noted before in studies with this probe (Allen et al., 1996).

The value of $\langle P_{2p} \rangle$ in activation is ~36% of the way from the relaxed to the rigor values. If the cross-bridges in active contraction were composed of a proportion of heads with the rigor disposition, and the rest were like relaxed cross-bridges, then the $\langle P_{2p} \rangle$ values might indicate that ~36% of the heads in activating solution are attached as in rigor. However $\langle P_{2s} \rangle$ and $\langle P_{4s} \rangle$ in activation do not lie between their relaxed and rigor values, a result incompatible with an active distribution comprising simply relaxed and rigor populations. The data suggest instead that active cross-bridges have a new orientation distribution, different from either the relaxed or rigor ones. Other data using probes at several sites on the RLC have also indicated a new distribution in active contraction (Sabido-David et al., 1998b; Hopkins et al., 1998).

Relationship to other studies

X-ray diffraction (HE Huxley et al., 1983; Lombardi et al., 1995; Dobbie et al., 1998; Linari et al., 2000), spectroscopic methods (Borejdo et al., 1982; Barnett and Thomas, 1989; Tanner et al., 1992; Hambly et al., 1992; Roopnarine and Thomas, 1995; Irving et al., 1995; Allen et al., 1996; Ling et al., 1996; Berger et al., 1996; Sabido-David et al., 1998; Corrie et al., 1999) and electron microscopy (Reedy et al., 1965; Pollard et al., 1993; Hirose et al., 1993; Lenart et al., 1996; Taylor et al., 1999) have been used extensively to detect tilting motions of myosin domains in muscle fibers. Most of these studies have shown that both the motor domain (MD) and the light chain domain (LCD) have broad orientation distributions in relaxation, narrower ones during contraction, and the narrowest orientation distribution in rigor.

The results of the present work are in general agreement these experiments, indicating that the degree of order in the angular distribution of the RLC is highest in rigor, intermediate in contraction and lowest in relaxation. The overall orientation distribution in activation is nearer to the relaxed condition than to rigor, consistent with a relatively small number of cross-bridges attached at any instant during contraction (Cooke et al., 1982; Baker et al., 1998; Hopkins et al., 1998, 2002; Ramachandran and Thomas, 1999; Corrie et al., 1999).

Hellen et al. (1995) have performed experiments on muscle fibers labeled with rhodamine at Cys^{707} resembling those in the present work. Their measurements correspond approximately to the ones here with *x* illumination, but with a longer (200 μs) photoselection pulse, and with the probe located in the motor domain. They detected rapid ($\ll$200 μs) motion of the probes in the MD in active contraction and relaxation, but less motion in rigor.

In scallop muscle, the transition from relaxation to active contraction is accompanied by a shift between two RLC orientations spaced 36° apart, but this shift is less prominent in rabbit skeletal muscle (Baker et al., 1998; Hopkins et al., 2002). To gain information on the microsecond time scale, saturation-transfer EPR (Roopnarine et al., 1998) and time-resolved phosphorescence anisotropy (TPA, Ramachandran and Thomas, 1999) have been applied to scallop myofibrils. These studies identified microsecond motions unique to active contraction, similar to those identified here. The TPA experiment identified components of motion in active contraction with correlation times of 5, 40, and 300 μs and a total amplitude of 40°. The slowest component comprised a relatively small proportion (24% of the anisotropy change, corresponding to 17% of the amplitude of the microsecond wobble). In the present work, we measured microsecond

motions of the RLC during isometric contraction of vertebrate muscle fibers. The amplitude of this motion during contraction is 48° when modeled as wobble in a cone, comparable to the amplitude of motion in scallop muscle. However, we did not observe any decay of anisotropy imposed by the bleaching pulse after the 20 μs instrument dead time, as would be expected from the small 300 μs component in scallop myofibrils (Ramachandran and Thomas, 1999). This difference may be inherent in the different muscle types or because the scallop myofibrils undergo extreme shortening in the contraction solution before the measurements are made (Ramachandran and Thomas, 1999). In the present work, the measurements are made under isometric conditions.

The millisecond recovery of tension following length steps in active muscle fibers (Huxley and Simmons, 1971; Lombardi et al., 1992; Martyn and Chase, 1995; Irving et al., 1995) also suggests that cross-bridges should exhibit components of motion slower than 20 μs. The present results, indicating that any motions slower than 20 μs are small in isometric fibers, may result from the long contractions required to collect the PFD data, the low temperature of the experiments (11°C) and, possibly, reduction of the amplitude of quick recovery by the RLC exchange procedure (Hopkins et al., 1998, 2002). Alternatively, tilting motions of the LCD on a time scale greater than 100 μs may be more closely related to filament sliding than to force generation (Ishii et al., 2001).

Summary

The method of polarized fluorescence depletion is presented and tested. It is capable of separating orientational dynamics in the μs time regime from static order, and supplies more highly resolved static orientational information than that available from conventional fluorescence polarization experiments. Rotational motions of the RLC occur over wide angular ranges in relaxed muscle and narrower ones in rigor. Microsecond motions of the RLC during contraction are sufficient to explain the increased breadth of the active orientation distribution relative to rigor. Thus dynamic motions of the RLC play a major role in the contraction mechanism.

APPENDIX

Expressions used to estimate order parameters of the probe orientation distribution in polarized fluorescence depletion experiments are derived. The derivation follows that of Dale et al. (1999) extended to the present case of transient removal by reversible bleaching of a proportion of the probe population. Some expressions (or their equivalents) from Dale et al. (1999) are repeated here for convenience and are designated, for example, as Eq. D.1 (Eq. 1 in Dale et al., 1999). The geometry and definitions of the angular quantities between excitation and emission propagation directions and polarizer angles are shown in Fig. A1. The absorption and emission dipole moments of the probes are assumed here to be collinear, as approximately applies to the rhodamine probe used in the present work (Chen and Bowman, 1965; Penzkofer and Wiedmann, 1980; Hopkins et al., 1998), but non-collinearity can also be treated (Londo et al., 1993; Dale et al., 1999). A general solution for the results expected from the PFD experiment based on the stated assumptions has been obtained using Wigner matrix algebra (available upon request from Y.E.G.). A trigonometric approach, based on the completion theorem, is detailed here.

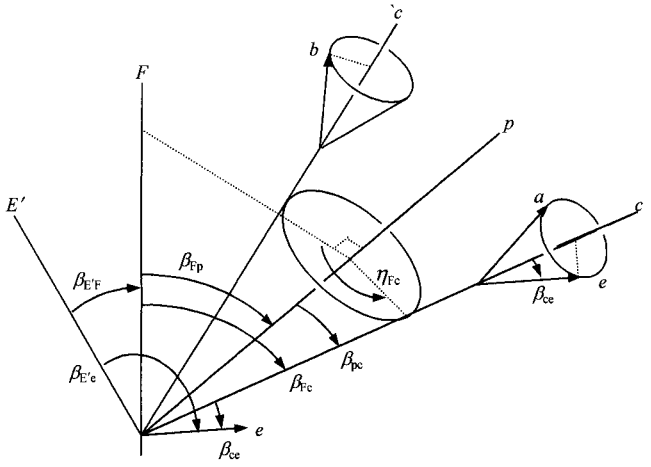

FIGURE A1 Relationships between the geometric axes relevant to the PFD experiment. F, muscle fiber axis, E', orientation of the polarization (electric field) of the photoselection bleaching pulse (the same as F in the present experiments). p, static protein axis for a particular molecule. c, the microsecond wobble axis. a and e, the fast wobbling probe absorption dipole moments. $`c$, microsecond wobble axis at the time of the bleach pulse. $b$, orientation of the absorption dipole moment at the time of the bleach pulse. Dipole $b$ is taken to diffuse about axis $`c$ with the same distribution as a about axis c.

Two types of motion are considered about an average orientation, p, that is static on the time scale of the measurement, 1 ms. The protein carrying the probe is taken to wobble with cylindrical symmetry about an axis, p, on a time scale 4 ns $\ll \tau_{wobble} \ll 1$ μs carrying the probe angle to positions given by axis, c. Very rapid motions, much faster than the fluorescence (singlet excited state) lifetime τ_f (e.g., ~4 ns for rhodamine) and having cylindrical symmetry about c, position the absorption and emission dipoles at a and e. A brief intense bleach pulse excites some of the probes into the triplet state where they do not contribute to fluorescence measured by a weak interrogation beam. Measurements of steady-state polarized fluorescence intensities before and after transient photobleaching lead to estimates for the extent of motion on both of these time scales and then to the orientation distribution with these motions removed.

Steady-state fluorescence polarization and fast wobble

Fluorescent probes bound to a protein within an organized macromolecular system, such as a muscle fiber or a bilayer membrane, undergo very fast wobble with a restricted amplitude. Under the following four conditions, Dale et al. (1999) presented a method to estimate the orientation distribution of the probe taking account of this wobble: 1) the wobble of the fluorescent probes with respect to the protein is fast relative to the decay time constant, τ_f, of the optically excited singlet state; 2) the angular distributions of the absorption and emission transition dipole moments attained during this rapid motion are cylindrically symmetric about an axis, c, and are independent of the orientation of c in the ordered system; 3) c is fixed within the protein and protein motions are negligible during the

lifetime of the excited state; and 4) the overall system under study exhibits cylindrical symmetry about its director (e.g., the fiber axis, F, oriented in the z axis of the laboratory coordinate frame). Several polarized fluorescence intensities, ${}_{m}I_{n}$, are measured along paths perpendicular to F, with polarizations either parallel or perpendicular to F. The subscript preceding each intensity indicates excitation polarization parallel or perpendicular to F; the trailing subscript indicates analyzer polarization parallel or perpendicular to F. The path of the detected beam is in the x axis (perpendicular to F). Superscripts preceding the intensities indicate the path of the excitation beam, x parallel or y perpendicular to the path of the detected beam. Because of the cylindrical symmetry of the sample around F, ${}_{\parallel}I_{\parallel} = {}^{x}_{\parallel}I_{\parallel} = {}^{y}_{\parallel}I_{\parallel}$. Moreover, for fluorophores with approximately collinear absorption and emission dipoles, such as rhodamine, ${}_{\perp}I_{\parallel} = {}_{\parallel}I_{\perp} = {}^{x}_{\perp}I_{\parallel} = {}^{y}_{\perp}I_{\parallel} = {}^{x}_{\parallel}I_{\perp} = {}^{y}_{\parallel}I_{\perp}$. These identities leave four independent intensities, ${}_{\parallel}I_{\parallel}$, ${}_{\perp}I_{\parallel}$, ${}^{x}_{\perp}I_{\perp}$, and ${}^{y}_{\perp}I_{\perp}$. Then the order parameters for the probe orientation distribution are given (Dale et al., 1999) by:

$$\langle P_{2d}\rangle = S_d + \sqrt{S_d^2 - G_0 + 6G_2} \qquad \text{(D.17)}$$

$$\langle P_2\rangle = \frac{S_d}{\langle P_{2d}\rangle} \qquad \text{(D.15)}$$

$$\langle P_4\rangle = \frac{5}{3}\cdot\frac{G_0 + G_2}{\langle P_{2d}\rangle^2} - \frac{2}{3}, \qquad \text{(D.16)}$$

where

$$S_d = \langle P_{2d}\rangle\langle P_2\rangle = \frac{{}_{\parallel}I_{\parallel} + {}_{\perp}I_{\parallel} - {}^{x}_{\perp}I_{\perp} - {}^{y}_{\perp}I_{\perp}}{I_0} \qquad \text{(D.23, D.24)}$$

$$G_0 = \langle P_{2d}\rangle^2\langle P_2^2(\cos\beta_{Fc})\rangle = \frac{1}{2}\cdot\frac{2{}_{\parallel}I_{\parallel} - 4{}_{\perp}I_{\parallel} + {}^{x}_{\perp}I_{\perp} + {}^{y}_{\perp}I_{\perp}}{I_0} \qquad \text{(D.25)}$$

$$G_2 = \langle P_{2d}\rangle^2\langle\tfrac{3}{8}\sin^4\beta_{Fc}\rangle = \frac{3}{2}\cdot\frac{{}^{x}_{\perp}I_{\perp} - {}^{y}_{\perp}I_{\perp}}{I_0} \qquad \text{(D.26)}$$

and

$$I_0 = {}_{\parallel}I_{\parallel} + 4{}_{\perp}I_{\parallel} + 2{}^{x}_{\perp}I_{\perp} + 2{}^{y}_{\perp}I_{\perp}. \qquad \text{(D.27)}$$

$\langle P_2\rangle$ and $\langle P_4\rangle$ are order parameters (coefficients of a series expansion using Legendre polynomials as basis functions) describing the distribution of orientations, β_{Fc}, of the axis, c, relative to F. $\langle P_2\rangle \equiv \langle P_2(\cos\beta_{Fc})\rangle$ and $\langle P_4\rangle \equiv \langle P_4(\cos\beta_{Fc})\rangle$, where the functions $P_2(\,)$ and $P_4(\,)$ are 2nd- and 4th-rank Legendre polynomials and the brackets, $\langle\,\rangle$, denote an ensemble average over the probability density function integrated over the whole angular range (i.e., over β in $[0, \pi]$). The wobble represented by $\langle P_{2d}\rangle$ occurs on a time-scale much faster than that of the fluorescence decay ($\tau_f \sim$ 4 ns for rhodamine). Both dynamic disorder of c with respect to p, caused by motions slower than the fluorescence decay, and static disorder of p with respect to F contribute to $\langle P_2\rangle$ and $\langle P_4\rangle$. The orientation distribution described by $\langle P_2\rangle$ and $\langle P_4\rangle$ thus has the sub-nanosecond motions removed or 'factored out' as in Eqs. D.15 and D.16. S_d, G_0 and G_2 are functions involving correlations between the dipole position at the moment of absorption and at that of emission. These correlation functions are mainly used as intermediates in obtaining the order parameters from the measured polarizations (Eqs. D.15–D.17).

Microsecond wobble detectable by polarized fluorescence depletion

Let the protein wobble on a slower timescale reorient the probe axis c cylindrically symmetrically around a static central axis, p. The relevant order parameters can be expressed in relationships containing both the extent of these intermediate time scale motions and the static orientation distribution. The geometrical assumptions for motions of c about p are similar to those made for the rapid motion of the dipoles about c (Dale et al., 1999 and listed above): the motions are cylindrically symmetric about their central axis, p, independent of the orientation of p with respect to the sample, and rapid enough to be effectively complete during the bleach period and before observation (Fig. A1). These assumptions imply that the intermediate time scale motions are independent of both faster subnanosecond probe motions and slower protein motions. Based on this independence and on the completion theorem (e.g. as used in Dale et al., 1999 for the fast wobble case), the ensemble order parameters can be separated into products as:

$$\langle P_2\rangle = \langle P_{2p}\rangle\langle P_{2s}\rangle \qquad \text{(A.1)}$$

$$\langle P_4\rangle = \langle P_{4p}\rangle\langle P_{4s}\rangle \qquad \text{(A.2)}$$

where the order parameters describing the microsecond rotational motions of the protein about the central axis p are $\langle P_{2p}\rangle \equiv \langle P_2(\cos\beta_{pc})\rangle$ and $\langle P_{4p}\rangle \equiv \langle P_4(\cos\beta_{pc})\rangle$, while the order parameters describing the orientation distribution function of p with respect to the sample axis F are $\langle P_{2s}\rangle \equiv \langle P_2(\cos\beta_{Fp})\rangle$ and $\langle P_{4s}\rangle \equiv \langle P_4(\cos\beta_{Fp})\rangle$. The relevant correlation functions (Eqs. D.23 to D.26 above), including the separation of the motions on the two time scales, are then:

$$S_d = \langle P_{2d}\rangle\langle P_{2p}\rangle\langle P_{2s}\rangle \qquad \text{(A.3)}$$

$$G_0 = \langle P_{2d}\rangle^2(\tfrac{1}{5} + \tfrac{2}{7}\langle P_{2p}\rangle\langle P_{2s}\rangle + \tfrac{18}{35}\langle P_{4p}\rangle\langle P_{4s}\rangle) \qquad \text{(A.4)}$$

$$G_2 = \langle P_{2d}\rangle^2(\tfrac{1}{5} - \tfrac{2}{7}\langle P_{2p}\rangle\langle P_{2s}\rangle + \tfrac{3}{35}\langle P_{4p}\rangle\langle P_{4s}\rangle). \qquad \text{(A.5)}$$

The expressions within the parentheses are equivalent for the present case to those obtained previously (Vogel and Jähnig, 1985) relating to the analogous nanosecond-timescale situation.

Order parameters and correlation functions after photobleaching

The static orientation distribution of a population or fluorophores transiently bleached by a brief photoselection pulse can be estimated in terms of order parameters up to at least $\langle P_{6s}\rangle$. Probe rotational motions between the bleach pulse and initiation of interrogation of the fluorophores remaining in the ground state, partially restore the pre-bleach distribution, and are described by $\langle P_{2p}\rangle$ and $\langle P_{4p}\rangle$. Thus order parameters and correlation functions for the bleached population, obtained in the PFD experiment, contain useful information beyond what is available from conventional (i.e., without bleaching) steady-state fluorescence polarization measurements.

For bleaching of only a small fraction of the total number of probes, the probability of bleaching a particular probe molecule is proportional to $(\grave{E}\cdot b)^2$, where $\grave{E}$ is a unit vector representing the direction of the electric field of the linearly polarized bleach beam (here parallel to F) and b is a unit vector representing the probe absorption transition dipole moment (Fig. A1). Here, b is the same absorption dipole as that represented by a in expressions for polarized fluorescence intensities (e.g. text Eq. 1), but separated in time between bleach and interrogation. Beginning at $t < 0$ corresponding to the bleach event, the wobbling protein axis is oriented at some arbitrary position, $\grave{c}$, within its distribution about p and it relaxes to another such position, c, at $t = 0$, the initial time of interrogation (Fig. A1).

The distribution of b about $\backslash c$ is identical to that of a and e about c, and since a and e are collinear,

$$\langle P_{2d}\rangle \equiv \langle P_2(\cos\beta_{ca})\rangle = \langle P_2(\cos\beta_{ce})\rangle = \langle P_2(\cos\beta_{\backslash cb})\rangle.$$

The bleach pulse is initially considered to have spatially uniform intensity. The fraction of bleached chromophores created by the bleach pulse is then given by the ensemble average $B\langle(\backslash E\cdot b)^2\rangle$, and the fraction remaining in the ground state by $1 - B\langle(\backslash E\cdot b)^2\rangle$, where B is a parameter proportional to the overall depth (extent) of bleaching. The polarized post-bleach fluorescence component ${}_{\backslash E,E}I_{E'}$ that arises from the remaining ground state fraction is given by taking the ensemble average over the product of $1 - B(\backslash E\cdot b)^2$ and $(E\cdot a)^2(E'\cdot e)^2$, including the appropriate scaling factor for total (independent of polarization) intensity, I_0:

$$\begin{aligned}{}_{\backslash E,E}I_{E'} &= I_0\langle[1 - B\cdot(\backslash E\cdot b)^2](E\cdot a)^2(E'\cdot e)^2\rangle\\ &= {}_{E}I_{E'} - {}_{\backslash E,E}\Delta_{E'}\end{aligned} \tag{A.6}$$

where ${}_{\backslash E,E}\Delta_{E'}$ represents the difference in pre- and post-bleach fluorescence. Thus:

$${}_{\backslash E,E}\Delta_{E'} = {}_{E}I_{E'} - {}_{\backslash E,E}I_{E'} = \frac{\Delta_0}{I_0}\frac{\langle(\backslash E\cdot b)^2{}_{E}I_{E'}\rangle}{\langle(\backslash E\cdot b)^2\rangle}, \tag{A.7}$$

where the total difference intensity Δ_0 (independent of polarization) is given, analogously to I_0 (Eq. D.27 above) by: $\Delta_0 = {}_{\parallel}\Delta_{\parallel} + 4\,{}_{\perp}\Delta_{\parallel} + 2{}^{x}_{\perp}\Delta_{\perp} + 2{}^{y}_{\perp}\Delta_{\perp} = I_0\langle B(\backslash E\cdot b)^2\rangle$, which, together with $\langle(\backslash E\cdot b)^2\rangle = \langle\cos^2\theta_{\backslash Eb}\rangle = \frac{1}{3}[1 + 2\langle P_2(\cos\theta_{\backslash Eb})\rangle] = \frac{1}{3}[1 + 2S_d]$, leads to a depth of bleaching given by:

$$B = \frac{3\Delta_0/I_0}{1 + 2S_d} \tag{A.8}$$

From equations A.7 (compare D.6 of Dale et al., 1999), the expression for the polarized difference intensities may be written:

$${}_{\backslash E,E}\Delta_{E'} = \frac{\Delta_0}{9}\left\{\begin{array}{l}1 + 2\{P_2(\cos\theta_{EF}) + P_2(\cos\theta_{E'F})\}S_d^B\\ \quad + 4\{P_2(\cos\theta_{EF})P_2(\cos\theta_{E'F})\}G_0^B\\ \quad + 3\{\sin^2\theta_{EF}\sin^2\theta_{E'F}\cos 2\xi_{EE'}\}G_2^B\end{array}\right\} \tag{A.9}$$

where θ_{EF} and $\theta_{E'F}$ are the angles made by the electric vectors of the excitation and emission, respectively, relative to F, and $\xi_{EE'}$ is their azimuth in the plane perpendicular to F (Fig. 1 of Dale et al., 1999). In the present case, the photobleaching pulse, $\backslash E$, is polarized parallel to the sample axis, F, which is aligned with the laboratory axis, z. With excitation light paths aligned along the x or y axes, emission along the x axis, polarizer angles either $\parallel$ or $\perp$ to F, and with the assumption of collinear absorption and emission dipoles, four independent polarized difference intensities ${}_{E}\Delta_{E'}$, are obtainable. These are given by inserting the appropriate angles into Eq. A.9:

$${}_{\parallel}\Delta_{\parallel} = \frac{\Delta_0}{9}(1 + 4S_d^B + 4G_0^B)$$

$${}_{\perp}\Delta_{\parallel} = \frac{\Delta_0}{9}(1 + S_d^B - 2G_0^B)$$

$${}^{x}_{\perp}\Delta_{\perp} = \frac{\Delta_0}{9}(1 - 2S_d^B + G_0^B + 3G_2^B)$$

$${}^{y}_{\perp}\Delta_{\perp} = \frac{\Delta_0}{9}(1 - 2S_d^B + G_0^B - 3G_2^B) \tag{A.10}$$

which can be inverted to give correlation functions of the bleached population based on the measured difference intensities:

$$S_d^B = \frac{{}_{\parallel}\Delta_{\parallel} + {}_{\perp}\Delta_{\parallel} - {}^{x}_{\perp}\Delta_{\perp} - {}^{y}_{\perp}\Delta_{\perp}}{\Delta_0} \tag{A.11}$$

$$G_0^B = \frac{1}{2}\cdot\frac{2{}_{\parallel}\Delta_{\parallel} - 4{}_{\perp}\Delta_{\parallel} + {}^{x}_{\perp}\Delta_{\perp} + {}^{y}_{\perp}\Delta_{\perp}}{\Delta_0} \tag{A.12}$$

$$G_2^B = \frac{3}{2}\cdot\frac{{}^{x}_{\perp}\Delta_{\perp} - {}^{y}_{\perp}\Delta_{\perp}}{\Delta_0} \tag{A.13}$$

with Δ_0 defined above.

From Eqs. A.7 and A.9, together with A.11 to A.13, and by analogy to the relationships for normal (no bleach) populations given in Eqs. A.1 to A.5, it is seen that these correlation functions may also be expressed as:

$$S_d^B = \frac{\langle(\backslash E\cdot b)^2 S_d\rangle}{\langle(\backslash E\cdot b)^2\rangle} = \langle P_{2d}^B\rangle\langle P_2^B\rangle \tag{A.14}$$

$$G_0^B = \frac{\langle(\backslash E\cdot b)^2 G_0\rangle}{\langle(\backslash E\cdot b)^2\rangle} = \langle P_{2d}^B\rangle^2(\tfrac{1}{5} + \tfrac{2}{7}\langle P_2^B\rangle + \tfrac{18}{35}\langle P_4^B\rangle) \tag{A.15}$$

$$G_2^B = \frac{\langle(\backslash E\cdot b)^2 G_2\rangle}{\langle(\backslash E\cdot b)^2\rangle} = \langle P_{2d}^B\rangle^2(\tfrac{1}{5} - \tfrac{2}{7}\langle P_2^B\rangle + \tfrac{3}{35}\langle P_4^B\rangle) \tag{A.16}$$

where $\langle P_2^B\rangle \equiv \langle P_2(\cos\beta_{Fc})\rangle_B$ and $\langle P_4^B\rangle \equiv \langle P_4(\cos\beta_{Fc})\rangle_B$ are bleached population order parameters describing the distribution of the angle, β_{Fc}, between the sample axis, F, and the probe central axis, c (Fig. A1), averaged over the bleached population.

As in the case of the correlation functions for the pre-bleach orientation distribution, Eqs. Eqs. A.14 to A.16 can be inverted to give

$$\langle P_{2d}^B\rangle = S_d^B + \sqrt{S_d^{B2} - G_0^B + 6G_2^B} \tag{A.17}$$

$$\langle P_2^B\rangle = \frac{S_d^B}{\langle P_{2d}^B\rangle} \tag{A.18}$$

$$\langle P_4^B\rangle = \frac{5}{3}\cdot\frac{G_0^B + G_2^B}{\langle P_{2d}^B\rangle^2} - \frac{2}{3} \tag{A.19}$$

Note the similarity between Eqs. A.11 to A.19 for the bleached population and Eqs. D.15 to D.27 for the entire probe population at steady state, and that $\langle P_{2d}^B\rangle = \langle P_{2d}\rangle$.

Calculation of microsecond motions and static order parameters

In the present work, $\backslash E$ is parallel to F, so that the denominator of the central expressions of Eqs. A.14 to A.16 is given by:

$$\begin{aligned}\langle(\backslash E\cdot b)^2\rangle &= \langle\tfrac{1}{3}(1 + 2P_2(\backslash E\cdot b))\rangle\\ &= \tfrac{1}{3}[1 + 2\langle P_2(\cos 0)\rangle\langle P_2(\cos\beta_{\backslash cb})\rangle\\ &\qquad\cdot\langle P_2(\cos\beta_{pc})\rangle\langle P_2(\cos\beta_{Fp})\rangle]\\ &= \tfrac{1}{3}[1 + 2\langle P_{2d}\rangle\langle P_{2p}\rangle\langle P_{2s}\rangle]\end{aligned} \tag{A.20}$$

The correlation functions for the bleached population can then also be expressed as:

$$S_d^B = \frac{\frac{1}{3}\langle(1 + 2\langle P_{2d}\rangle\langle P_{2p}\rangle P_{2s})S_d\rangle}{\frac{1}{3}(1 + 2\langle P_{2d}\rangle\langle P_{2p}\rangle\langle P_{2s}\rangle)}$$

$$= \frac{S_d + 2\langle P_{2d}\rangle^2\langle P_{2,2}\rangle}{1 + 2\langle P_{2d}\rangle\langle P_2\rangle} \quad (A.21)$$

$$G_0^B = \frac{\frac{1}{3}\langle(1 + 2\langle P_{2d}\rangle\langle P_{2p}\rangle P_{2s})G_0\rangle}{\frac{1}{3}(1 + 2\langle P_{2d}\rangle\langle P_{2p}\rangle\langle P_{2s}\rangle)}$$

$$= \frac{G_0 + 2\langle P_{2d}\rangle^3(\frac{1}{5}\langle P_2\rangle + \frac{2}{7}\langle P_{2,2}\rangle + \frac{18}{35}\langle P_{4,2}\rangle)}{1 + 2\langle P_{2d}\rangle\langle P_2\rangle} \quad (A.22)$$

$$G_2^B = \frac{\frac{1}{3}\langle(1 + 2\langle P_{2d}\rangle\langle P_{2p}\rangle P_{2s})G_2\rangle}{\frac{1}{3}(1 + 2\langle P_{2d}\rangle\langle P_{2p}\rangle\langle P_{2s}\rangle)}$$

$$= \frac{G_2 + 2\langle P_{2d}\rangle^3(\frac{1}{5}\langle P_2\rangle - \frac{2}{7}\langle P_{2,2}\rangle + \frac{3}{35}\langle P_{4,2}\rangle)}{1 + 2\langle P_{2d}\rangle\langle P_2\rangle}. \quad (A.23)$$

Here, $\langle P_{2,2}\rangle$ and $\langle P_{4,2}\rangle$ in Eqs. A.21–A.23 are parameters related to correlations of two-photon and three-photon events, respectively, and are dependent on intermediate time scale motions and the static orientation distribution. They are defined as:

$$\langle P_{2,2}\rangle \equiv \langle P_{2p}\rangle^2\langle P_{2s}P_{2s}\rangle$$

$$= \langle P_{2p}\rangle^2(\tfrac{1}{5} + \tfrac{2}{7}\langle P_{2s}\rangle + \tfrac{18}{35}\langle P_{4s}\rangle) \quad (A.24)$$

and:

$$\langle P_{4,2}\rangle \equiv \langle P_{4p}\rangle\langle P_{2p}\rangle\langle P_{4s}P_{2s}\rangle$$

$$= \langle P_{4p}\rangle\langle P_{2p}\rangle(\tfrac{2}{7}\langle P_{2s}\rangle + \tfrac{20}{77}\langle P_{4s}\rangle + \tfrac{5}{11}\langle P_{6s}\rangle) \quad (A.25)$$

$\langle P_{4,2}\rangle$ is a "triple correlation order parameter" involving all three photonic events in the PFD experiment: photoselection of the bleached population, absorption of a photon during the interrogation phase, and fluorescence emission. It depends on the static orientational distribution out to the 6th rank, $\langle P_{6s}\rangle \equiv \langle P_6(\cos\beta_{Fp})\rangle$, and the microsecond-dynamic distribution out to the 4th rank, $\langle P_{4p}\rangle \equiv \langle P_4(\cos\beta_{pc})\rangle$, neither of which is available via conventional (no bleaching) fluorescence polarization measurements.

$\langle P_{2,2}\rangle$ and $\langle P_{4,2}\rangle$ are also related to the order parameters for the bleached and unbleached populations. Comparison of Eqs. A.3 to A.5 with Eqs. A.14 to A.16, respectively, recalling also that $\langle P_{2d}^B\rangle = \langle P_{2d}\rangle$ and $\langle(\grave{E}\cdot b)^2\rangle = \frac{1}{3}(1 + 2S_d)$, leads to:

$$\langle P_2^B\rangle = \frac{\langle(\grave{E}\cdot b)^2P_2\rangle}{\langle(\grave{E}\cdot b)^2\rangle} = \frac{\langle(1 + 2\langle P_{2d}\rangle\langle P_{2p}\rangle P_{2s})P_2\rangle}{(1 + 2\langle P_{2d}\rangle\langle P_{2p}\rangle\langle P_{2s}\rangle)}$$

$$= \frac{\langle P_2\rangle + 2\langle P_{2d}\rangle\langle P_{2,2}\rangle}{1 + 2S_d} \quad (A.26)$$

and:

$$\langle P_4^B\rangle = \frac{\langle(\grave{E}\cdot b)^2P_4\rangle}{\langle(\grave{E}\cdot b)^2\rangle} = \frac{\langle(1 + 2\langle P_{2d}\rangle\langle P_{2p}\rangle P_{2s})P_4\rangle}{(1 + 2\langle P_{2d}\rangle\langle P_{2p}\rangle\langle P_{2s}\rangle)}$$

$$= \frac{\langle P_4\rangle + 2\langle P_{2d}\rangle\langle P_{4,2}\rangle}{1 + 2S_d} \quad (A.27)$$

and to expressions for $\langle P_{2,2}\rangle$ and $\langle P_{4,2}\rangle$ in terms of quantities obtainable from the experimental steady-state and difference intensities:

$$\langle P_{2,2}\rangle = \frac{\langle P_2^B\rangle(1 + 2S_d) - \langle P_2\rangle}{2\langle P_{2d}\rangle}$$

and

$$\langle P_{4,2}\rangle = \frac{\langle P_4^B\rangle(1 + 2S_d) - \langle P_4\rangle}{2\langle P_{2d}\rangle}. \quad (A.28)$$

Eqs. A.1 and A.2 together with A.24 and A.25 contain five new unknown quantities, $\langle P_{2p}\rangle$, $\langle P_{4p}\rangle$, $\langle P_{2s}\rangle$, $\langle P_{4s}\rangle$ and $\langle P_{6s}\rangle$, whereas only four independent parameters, $\langle P_2\rangle$, $\langle P_4\rangle$, $\langle P_{2,2}\rangle$ and $\langle P_{4,2}\rangle$, are experimentally determinable from PFD. Thus, all five of the unknown quantities cannot be uniquely determined. However, the relationship between $\langle P_{2p}\rangle$ and $\langle P_{4p}\rangle$ is determined solely by the shape of the angular distribution occupied during the microsecond time scale wobble. If we assume that this distribution can be described by equal probability within a cone of half-angle, δ_p, (wobble-in-cone model, Kinosita et al., 1977), then

$$\langle P_{2p}(\delta_p)\rangle = \tfrac{1}{2}\cos\delta_p(1 + \cos\delta_p)$$

$$\langle P_{4p}(\delta_p)\rangle = \tfrac{1}{8}\cos\delta_p(1 + \cos\delta_p)(7\cos^2\delta_p - 3) \quad (A.29)$$

and δ_p, $\langle P_{2s}\rangle$, $\langle P_{4s}\rangle$ and $\langle P_{6s}\rangle$ can be determined independently from the difference intensity data using Eqs. A.11 to A.13, A.17 to A.19, A.24, A.25 and A.28, with $\langle P_{2d}\rangle$, $\langle P_2\rangle$ and $\langle P_4\rangle$ having been determined from the steady-state fluorescence data (without bleaching). Other choices for the shape of the microsecond wobble distribution, such as a cylindrically symmetrical Gaussian spread about a central peak or diffusion around the periphery of a cone, give similar relationships and results.

High-bleach modifications

The expressions given thus far have assumed that bleaching is proportional to $\cos^2(\grave{E}\cdot b)$, as expected at low bleach depths. As bleach depth increases, however, the bleaching function becomes "flattened" as it becomes saturated at small angles (Axelrod et al., 1976; Hellen and Burghardt, 1994). The fraction of fluorophores remaining in the ground state after a bleach pulse having a spatially uniform intensity profile is given in general by $\langle\exp(-B\cdot(\grave{E}\cdot b)^2)\rangle$, and the bleached fraction is thus $\langle 1 - \exp(-B\cdot(\grave{E}\cdot b)^2)\rangle$ (Dale, 1987). Taking the first two terms of a Taylor series expansion of the exponential function to correct the previous expressions for a larger bleach depth and deriving the equivalent of the bleached correlation functions (A.21 to A.23) as before leads to:

$$S_d^B(B) \approx \frac{S_d + 2S_d^d - \frac{3B}{70}(7S_d + 20S_d^d + 8S_d^t)}{1 + 2S_d - \frac{3B}{70}(7 + 20S_d + 8\langle P_{4d}\rangle\langle P_4\rangle)} \quad (A.30)$$

$$G_0^B(B) \approx \frac{G_0 + 2G_0^t - \frac{3B}{70}(7G_0 + 20G_0^t + 8G_0^q)}{1 + 2S_d - \frac{3B}{70}(7 + 20S_d + 8\langle P_{4d}\rangle\langle P_4\rangle)} \quad (A.31)$$

$$G_2^B(B) \approx \frac{G_2 + 2G_2^t - \frac{3B}{70}(7G_2 + 20G_2^t + 8G_2^q)}{1 + 2S_d - \frac{3B}{70}(7 + 20S_d + 8\langle P_{4d}\rangle\langle P_4\rangle)} \quad (A.32)$$

where

$$S_d^q = \langle P_{2d}\rangle^2\langle P_{2,2}\rangle,\ S_d^t = \langle P_{4d}\rangle\langle P_{2d}\rangle\langle P_{4,2}\rangle$$

$$G_0^t = \langle P_{2d}\rangle^3\left(\tfrac{1}{5}\langle P_2\rangle + \tfrac{2}{7}\langle P_{2,2}\rangle + \tfrac{18}{35}\langle P_{4,2}\rangle\right),$$

$$G_2^t = \langle P_{2d}\rangle^3\left(\tfrac{1}{5}\langle P_2\rangle - \tfrac{2}{7}\langle P_{2,2}\rangle + \tfrac{3}{35}\langle P_{4,2}\rangle\right),$$

$$G_0^q = \langle P_{4d}\rangle\langle P_{2d}\rangle^2\left(\tfrac{1}{5}\langle P_4\rangle + \tfrac{2}{7}\langle P_{4,2}\rangle + \tfrac{18}{35}\langle P_{4,4}\rangle\right)$$

and

$$G_2^q = \langle P_{4d}\rangle\langle P_{2d}\rangle^2\left(\tfrac{1}{5}\langle P_4\rangle - \tfrac{2}{7}\langle P_{4,2}\rangle + \tfrac{3}{35}\langle P_{4,4}\rangle\right) \quad (A.33)$$

$\langle P_{4,4}\rangle$ depends on the static orientational distribution out to the 8th rank, i.e., $\langle P_{8s}\rangle \equiv \langle P_8(\cos\beta_{Fp})\rangle$, as well as on the nanosecond-dynamic and microsecond-dynamic distributions out to the 4th rank, e.g., on $\langle P_{4d}\rangle \equiv \langle P_4(\cos\beta_{ca})\rangle = \langle P_4(\cos\beta_{ce})\rangle = \langle P_4(\cos\beta_{cb})\rangle$ for the nanosecond motion. Order parameters $\langle P_{4d}\rangle$ and $\langle P_{4,4}\rangle$ do not contribute in the limit of low bleaching depth. The total difference intensity, $\Delta_0(B)$ corresponding to Eq. A.8, is modified to:

$$\Delta_0(B) = I_0\langle 1 - \exp(-B(\mathit{E}\cdot b)^2)\rangle \approx I_0\frac{B}{3}\left[1 + 2S_d - \frac{3B}{70}(7 + 20S_d + 8\langle P_{4d}\rangle\langle P_4\rangle)\right] \quad (A.34)$$

and the depth of bleaching B is now given approximately by:

$$B \approx \frac{35}{3}\,\frac{1 + 2S_d - \sqrt{(1 + 2S_d)^2 - \frac{18}{35}\frac{\Delta_0(B)}{I_0}(7 + 20S_d + 8\langle P_{4d}\rangle\langle P_4\rangle)}}{7 + 20S_d + 8\langle P_{4d}\rangle\langle P_4\rangle}. \quad (A.35)$$

If the intensity profile of the bleaching beam is Gaussian rather than uniform, expressions A.30 to A.32 are altered by replacing each incidence of $(3B/70)$ by $B/35$, and there is a corresponding slight change in the definition of B and $\Delta_0(B)$. Derivations of these relationships are available by request (from Y.E.G.). Experimentally measured bleached population correlation functions are plotted vs. B in Fig. 11 of Results. Eqs. A.30 to A.32 and A.34 are fitted to those data to obtain the higher-rank order parameters and to extrapolate the values of the correlation functions to zero bleach.

We are grateful to Dr. John E.T. Corrie for kindly supplying the 6-IATR rhodamine probe and for helpful comments on the manuscript. We thank Drs. Henry Shuman, Jody Dantzig, Joe Forkey, and Malcolm Irving for useful discussions and suggestions, Mr. Perry Sun for the muscle fiber preparation, Dr. Martin Pring for advice regarding error estimates, Mr. Joe Pili for expert mechanical construction and Ms. Kimberly Vanzi for help preparing the manuscript. This work was supported by NIH grant R01-AR26846 and training grant GM08275.

REFERENCES

Adhikari, B., K. Hideg, and P. G. Fajer. 1997. Independent mobility of catalytic and regulatory domains of myosin heads. *Proc. Natl. Acad. Sci. U.S.A.* 94:9643–9647.

Allen, T. St. C., N. Ling, M. Irving, and Y. E. Goldman. 1996. Orientation changes in myosin regulatory light chains following photorelease of ATP in skinned muscle fibers. *Biophys. J.* 70:1847–1862.

Axelrod, D., D. E. Koppel, J. Schlessinger, E. Elson, and W. W. Webb. 1976. Mobility measurement by analysis of fluorescence photobleaching recovery kinetics. *Biophys. J.* 16:1055–1069.

Baker, J. E., I. Brust-Mascher, S. Ramachandran, L. E. W. LaConte, and D. D. Thomas. 1998. A large and distinct rotation of the myosin light chain domain occurs upon muscle contraction. *Proc. Natl. Acad. Sci. U.S.A.* 95:2944–2949.

Ballard, S. G. 1983. Normally on fast-gain switch for photomultiplier tubes. *Rev. Sci. Instrum.* 54:1473–1475.

Barnett, V. A., and D. D. Thomas. 1984. Saturation transfer electron paramagnetic resonance of spin-labeled muscle fibers. *J. Mol. Biol.* 179:83–102.

Barnett, V. A., and D. D. Thomas. 1989. Microsecond rotational motion of spin-labeled myosin heads during isometric muscle contraction. *Biophys. J.* 56:517–523.

Bell, M. G., R. E. Dale, U. A. van der Heide, and Y. E. Goldman. 2000. Polarized fluorescence depletion reports orientation distribution and rotational dynamics of muscle cross-bridges. *Biophys. J.* 78:120A.

Berger, C. L., J. S. Craik, D. R. Trentham, J. E. T. Corrie, and Y. E. Goldman. 1996. Fluorescence polarization of skeletal muscle fibers labeled with rhodamine isomers on the myosin heavy chain. *Biophys. J.* 71:3330–3343.

Berger, C. L., and D. D. Thomas. 1993. Rotational dynamics of actin-bound myosin heads in active myofibrils. *Biochemistry.* 32:3812–3821.

Borejdo, J., O. Assulin, T. Ando, and S. Putnam. 1982. Cross-bridge orientation in skeletal muscle measured by linear dichroism of an extrinsic chromophore. *J. Mol. Biol.* 158:391–414.

Burghardt, T. P., S. P. Garamszegi, and K. Ajtai. 1997. Probes bound to myosin Cys-707 rotate during length transients in contraction. *Proc. Natl. Acad. Sci. U.S.A.* 94:9631–9636.

Calhoun, D. B., J. M. Vanderkooi, G. V. Woodrow, III, and S. W. Englander. 1983. Penetration of dioxygen into proteins studied by quenching of phosphorescence and fluorescence. *Biochemistry.* 22: 1526–1532.

Chen, R. F., and R. L. Bowman. 1965. Fluorescence polarization: measurement with ultraviolet-polarizing filters in a spectrophotofluorometer. *Science.* 147:729–732.

Cooke, R. 1981. Stress does not alter the conformation of a domain of the myosin cross-bridge in rigor muscle fibres. *Nature.* 294:570–571.

Cooke, R. 1986. The mechanism of muscle contraction. *CRC Crit. Rev. Biochem.* 21:53–118.

Cooke, R., M. S. Crowder, and D. D. Thomas. 1982. Orientation of spin labels attached to cross-bridges in contracting muscle fibres. *Nature.* 300:776–778.

Corin, A. F., E. Blatt, and T. M. Jovin. 1987. Triplet-state detection of labeled proteins using fluorescence recovery spectroscopy. *Biochemistry.* 26:2207–2217.

Corrie, J. E. T., B. D. Brandmeier, R. E. Ferguson, D. R. Trentham, J. Kendrick-Jones, S. C. Hopkins, U. A. van der Heide, Y. E. Goldman, C. Sabido-David, R. E. Dale, S. Criddle, and M. Irving. 1999. Dynamic

measurement of myosin light-chain-domain tilt and twist in muscle contraction. *Nature.* 400:425–430.

Corrie, J. E. T., and J. S. Craik. 1994. Synthesis and characterisation of pure isomers of iodoacetamidotetramethylrhodamine. *J. Chem. Soc. Perkin Trans. 1.* 2967–2973.

Dale, R. E. 1987. Depolarized fluorescence photobleaching recovery. *Eur. Biophys. J.* 14:179–193.

Dale, R. E., S. C. Hopkins, U. A. van der Heide, T. Marszałek, M. Irving, and Y. E. Goldman. 1999. Model-independent analysis of the orientation of fluorescent probes with restricted mobility in muscle fibers. *Biophys. J.* 76:1606–1618.

Dobbie, I., M. Linari, G. Piazzesi, M. Reconditi, N. Koubassova, M. A. Ferenczi, V. Lombardi, and M. Irving. 1998. Elastic bending and active tilting of myosin heads during muscle contraction. *Nature.* 396:383–387.

Dobrowolski, Z., G-Q. Xu, and S. E. Hitchcock-DeGregori. 1991. Modified calcium-dependent regulatory function of troponin C central helix mutants. *J. Biol. Chem.* 266:5703–5710.

Dominguez, R., Y. Freyzon, K. M. Trybus, and C. Cohen. 1998. Crystal structure of a vertebrate smooth muscle myosin motor domain and its complex with the essential light chain: visualization of the pre-power stroke state. *Cell.* 94:559–571.

Fajer, P. G., E. A. Fajer, and D. D. Thomas. 1990. Myosin heads have a broad orientational distribution during isometric muscle contraction: time-resolved EPR studies using caged ATP. *Proc. Natl. Acad. Sci. U.S.A.* 87:5538–5542.

Fisher, A. J., C. A. Smith, J. B. Thoden, R. Smith, K. Sutoh, H. M. Holden, and I. Rayment. 1995. X-ray structures of the myosin motor domain of *Dictyostelium discoideum* complexed with MgADP · BeF_x and MgADP · AlF_4^-. *Biochemistry.* 34:8960–8972.

Geeves, M. A., and K. C. Holmes. 1999. Structural mechanism of muscle contraction. *Annu. Rev. Biochem.* 68:687–728.

Goldman, Y. E. 1998. Wag the tail: structural dynamics of actomyosin. *Cell.* 93:1–4.

Goldman, Y. E., M. G. Hibberd, and D. R. Trentham. 1984. Relaxation of rabbit psoas muscle fibers from rigor by photochemical generation of adenosine-5′-triphosphate. *J. Physiol.* 354:577–604.

Goldman, Y. E., and R. M. Simmons. 1984. Control of sarcomere length in skinned muscle fibres of *Rana temporaria* during mechanical transients. *J. Physiol.* 350:497–518.

Hambly, B., K. Franks, and R. Cooke. 1992. Paramagnetic probes attached to a light chain on the myosin head are highly disordered in active muscle fibers. *Biophys. J.* 63:1306–1313.

Hellen, E. H., K. Ajtai, and T. P. Burghardt. 1995. Myosin head rotation in muscle fibers measured using polarized fluorescence photobleaching recovery. *J. Fluorescence.* 5:355–367.

Hellen, E. H., and T. P. Burghardt. 1994. Saturation effects in polarized fluorescence photobleaching recovery and steady state fluorescence polarization. *Biophys. J.* 66:891–897.

Highsmith, S., and D. Eden. 1986. Myosin subfragment 1 has tertiary structural domains. *Biochemistry.* 25:2237–2242.

Hirose, K., T. D. Lenart, J. M. Murray, C. Franzini-Armstrong, and Y. E. Goldman. 1993. Flash and smash: rapid freezing of muscle fibers activated by photolysis of caged ATP. *Biophys. J.* 65:397–408.

Hopkins, S. C., C. Sabido-David, U. A. van der Heide, R. E. Ferguson, B. D. Brandmeier, R. E. Dale, J. Kendrick-Jones, J. E. T. Corrie, D. R. Trentham, M. Irving, and Y. E. Goldman. 2002. Orientation changes of the myosin light-chain-domain during filament sliding in active and rigor muscle. *J. Mol. Biol.* In press.

Hopkins, S. C., C. Sabido-David, J. E. T. Corrie, M. Irving, and Y. E. Goldman. 1998. Fluorescence polarization transients from rhodamine isomers on the myosin regulatory light chain in skeletal muscle fibers. *Biophys. J.* 74:3093–3110.

Houdusse, A., V. N. Kalabokis, D. Himmel, A. G. Szent-Györgyi, and C. Cohen. 1999. Atomic structures of scallop myosin subfragment S1 complexed with MgADP: a novel conformation of the myosin head. *Cell.* 97:459–470.

Huxley, A. F., and R. M. Simmons. 1971. Proposed mechanism of force generation in striated muscle. *Nature.* 233:533–538.

Huxley, H. E., and W. Brown. 1967. The low-angle X-ray diagram of vertebrate muscle and its behaviour during contraction and rigor. *J. Mol. Biol.* 30:383–434.

Huxley, H. E., and M. Kress. 1985. Crossbridge behaviour during muscle contraction. *J. Muscle Res. Cell Motil.* 6:153–161.

Huxley, H. E., R. M. Simmons, A. R. Faruqi, M. Kress, J. Bordas, and M. H. J. Koch. 1983. Changes in the x-ray reflections from contracting muscle during rapid mechanical transients and their structural implications. *J. Mol. Biol.* 169:469–506.

Irving, M., T. St. C. Allen, C. Sabido-David, J. S. Craik, B. Brandmeier, J. Kendrick-Jones, J. E. T. Corrie, D. R. Trentham, and Y. E. Goldman. 1995. Tilting of the light-chain region of myosin during step length changes and active force generation in skeletal muscle. *Nature.* 375: 688–691.

Ishii, Y., A. Ishijima, and T. Yanagida. 2001. Single molecule nanomanipulation of biomolecules. *Trends Biotechnol.* 19:211–216.

Johnson, P., and P. B. Garland. 1981. Depolarization of fluorescence depletion. A microscopic method for measuring rotational diffusion of membrane proteins on the surface of a single cell. *FEBS Lett.* 132: 252–256.

Johnson, P., and P. B. Garland. 1982. Fluorescent triplet probes for measuring the rotational diffusion of membrane proteins. *Biochem. J.* 203:313–321.

Kao, H. P., and A. S. Verkman. 1996. Construction and performance of a photobleaching recovery apparatus with microsecond time resolution. *Biophys. Chem.* 59:203–210.

Kinosita, K., Jr., S. Kawato, and A. Ikegami. 1977. A theory of fluorescence polarization decay in membranes. *Biophys. J.* 20:289–305.

Kume, H. 1994. Photomultiplier Tube, Principle to Application. Hamamatsu Photonics, Bridgewater, NJ. 135.

Lenart, T. D., J. M. Murray, C. Franzini-Armstrong, and Y. E. Goldman. 1996. Structure and periodicities of cross-bridges in relaxation, in rigor, and during contractions initiated by photolysis of caged Ca^{2+}. *Biophys. J.* 71:2289–2306.

Linari, M., G. Piazzesi, I. Dobbie, N. Koubassova, M. Reconditi, T. Narayanan, O. Diat, M. Irving, and V. Lombardi. 2000. Interference fine structure and sarcomere length dependence of the axial X-ray pattern from active single muscle fibres. *Proc. Natl. Acad. Sci. U.S.A.* 97: 7226–7231.

Ling, N., C. Shrimpton, J. Sleep, J. Kendrick-Jones, and M. Irving. 1996. Fluorescent probes of the orientation of myosin regulatory light chains in relaxed, rigor, and contracting muscle. *Biophys. J.* 70:1836–1846.

Lombardi, V., G. Piazzesi, M. A. Ferenczi, H. Thirlwell, I. Dobbie, and M. Irving. 1995. Elastic distortion of myosin heads and repriming of the working stroke in muscle. *Nature.* 374:553–555.

Lombardi, V., G. Piazzesi, and M. Linari. 1992. Rapid regeneration of the actin-myosin power stroke in contracting muscle. *Nature.* 355:638–641.

Londo, T. R., N. A. Rahman, D. A. Roess, and B. G. Barisas. 1993. Fluorescence depletion measurements in various experimental geometries provide true emission and absorption anisotropies for the study of protein rotation. *Biophys. Chem.* 48:241–257.

Ludescher, R. D., and D. D. Thomas. 1988. Microsecond rotational dynamics of phosphorecent-labeled muscle cross-bridges. *Biochemistry.* 27:3343–3351.

Martyn, D. A., and P. B. Chase. 1995. Faster force transient kinetics at submaximal Ca^{2+} activation of skinned psoas fibers from rabbit. *Biophys. J.* 68:235–242.

Mendelson, R. A., D. K. Schneider, and D. B. Stone. 1996. Conformations of myosin subfragment 1 ATPase intermediates from neutron and x-ray scattering. *J. Mol. Biol.* 256:1–7.

Michl, J., and E. W. Thulstrup. 1986. Solute alignment by photoselection, in liquid crystals, polymers, and membranes. *In* Spectroscopy with Polarized Light. VCH Publishers Inc., Deerfield Beach, FL. 192–194.

Milligan, R. A., and P. F. Flicker. 1987. Structural relationship of actin, myosin, and tropomyosin revealed by cryo-electron microscopy. *J. Cell Biol.* 105:29–39.

Penzkofer, A., and J. Wiedmann. 1980. Orientation of transition dipole moments of rhodamine 6G determined by excited state absorption. *Optics Commun.* 35:81–86.

Pollard, T. D., D. Bhandari, P. Maupin, D. Wachsstock, A. G. Weeds, and H. G. Zot. 1993. Direct visualization by electron microscopy of the weakly bound intermediates in the actomyosin adenosine triphosphatase cycle. *Biophys. J.* 64:454–471.

Rahman, N. A., I. Pecht, D. A. Roess, and B. G. Barisas. 1992. Rotational dynamics of type I Fc_E receptors on individually-selected rat mast cells studied by polarized fluorescence depletion. *Biophys. J.* 61:334–346.

Ramachandran, S., and D. D. Thomas. 1999. Rotational dynamics of the regulatory light chain in scallop muscle detected by time-resolved phosphorescence anisotropy. *Biochemistry.* 38:9097–9104.

Rayment, I., H. M. Holden, M. Whittaker, C. B. Yohn, M. Lorenz, K. C. Holmes, and R. A. Milligan. 1993a. Structure of the actin-myosin complex and its implications for muscle contraction. *Science.* 261: 58–65.

Rayment, I., W. R. Rypniewski, K. Schmidt-Bäse, R. Smith, D. R. Tomchick, M. M. Benning, D. A. Winkelmann, G. Wesenberg, and H. M. Holden. 1993b. Three-dimensional structure of myosin subfragment-1: a molecular motor. *Science.* 261:50–58.

Reedy, M. K., K. C. Holmes, and R. T. Tregear. 1965. Induced changes in orientation of the cross-bridges of glycerinated insect flight muscle. *Nature.* 207:1276–1280.

Roopnarine, O., A. G. Szent-Györgyi, and D. D. Thomas. 1998. Microsecond rotational dynamics of spin-labeled myosin regulatory light chain induced by relaxation and contraction of scallop muscle. *Biochemistry.* 37:14428–14436.

Sabido-David, C., B. Brandmeier, J. S. Craik, J. E. T. Corrie, D. R. Trentham, and M. Irving. 1998a. Steady-state fluorescence polarization studies of the orientation of myosin regulatory light chains in single skeletal muscle fibers using pure isomers of iodoacetamidotetramethylrhodamine. *Biophys. J.* 74:3083–3092.

Sabido-David, C., S. C. Hopkins, L. D. Saraswat, S. Lowey, Y. E. Goldman, and M. Irving. 1998b. Orientation changes of fluorescent probes at five sites on the myosin regulatory light chain during contraction of single skeletal muscle fibres. *J. Mol. Biol.* 279:387–402.

Savitzky, A., and M. J. E. Golay. 1964. Smoothing and differentiation of data by simplified least squares procedures. *Analyt. Chem.* 36: 1627–1639.

Shih, W. M., Z. Gryczynski, J. R. Lakowicz, and J. A. Spudich. 2000. A FRET-based sensor reveals large ATP hydrolysis-induced conformational changes and three distinct states of the molecular motor myosin. *Cell.* 102:683–694.

Smith, C. A., and I. Rayment. 1996. X-ray structure of the magnesium (II) ADP vanadate complex of the *Dictyostelium discoideum* myosin motor domain to 1.9 Å resolution. *Biochemistry.* 35:5404–5417.

Stein, R. A., R. D. Ludescher, P. S. Dahlberg, P. G. Fajer, R. L. H. Bennett, and D. D. Thomas. 1990. Time-resolved rotational dynamics of phosphorescent-labeled myosin heads in contracting muscle fibers. *Biochemistry.* 29:10023–10031.

Suzuki, Y., T. Yasunaga, R. Ohkura, T. Wakabayashi, and K. Sutoh. 1998. Swing of the lever arm of a myosin motor at the isomerization and phosphate-release steps. *Nature.* 396:380–383.

Takeuchi, S., and T. Nagai. 1985. Low power photomultiplier base circuit. *IEEE Trans. Nuclear Sci.* NS-32:78–81.

Tanner, J. W., D. D. Thomas, and Y. E. Goldman. 1992. Transients in orientation of a fluorescent cross-bridge probe following photolysis of caged nucleotides in skeletal muscle fibres. *J. Mol. Biol.* 223:185–203.

Taylor, K. A., H. Schmitz, M. C. Reedy, Y. E. Goldman, C. Franzini-Armstrong, H. Sasaki, R. T. Tregear, K. Poole, C. Lucaveche, R. J. Edwards, L. F. Chen, H. Winkler, and M. K. Reedy. 1999. Tomographic 3D reconstruction of quick-frozen, Ca^{2+}-activated contracting insect flight muscle. *Cell.* 99:421–431.

Thomas, D. D., and R. Cooke. 1980. Orientation of spin-labeled myosin heads in glycerinated muscle fibers. *Biophys. J.* 32:891–906.

Thomas, D. D., S. Ishiwata, J. Seidel, and J. Gergely. 1980. Submillisecond rotational dynamics of spin-labeled myosin heads in myofibrils. *Biophys. J.* 32:873–890.

Thomas, D. D., S. Ramachandran, O. Roopnarine, D. W. Hayden, and E. M. Ostap. 1995. The mechanism of force generation in myosin: a disorder-to-order transition, coupled to internal structural changes. *Biophys. J.* 68:135s–141s.

Tsaturyan, A. K., S. Y. Bershitksy, R. Burns, and M. A. Ferenczi. 1999. Structural changes in the actin-myosin cross-bridges associated with force generation induced by temperature jump in permeabilized frog muscle fibers. *Biophys. J.* 77:354–372.

Van der Heide, U. A., S. C. Hopkins, and Y. E. Goldman. 2000. A maximum entropy analysis of protein orientations using fluorescence polarization data from multiple probes. *Biophys. J.* 78:2138–2150.

Vibert, P., and C. Cohen. 1988. Domains, motions and regulation in the myosin head. *J. Muscle Res. Cell Motil.* 9:296–305.

Vogel, H., and F. Jähnig. 1985. Fast and slow orientational fluctuations in membranes. *Proc. Natl. Acad. Sci. U.S.A.* 82:2029–2033.

Wakabayashi, K., M. Tokunaga, I. Kohno, Y. Sugimoto, T. Hamanaka, Y. Takezawa, T. Wakabayashi, and Y. Amemiya. 1992. Small-angle synchrotron x-ray scattering reveals distinct shape changes of the myosin head during hydrolysis of ATP. *Science.* 258:443–447.

Yoshida, T. M., and B. G. Barisas. 1986. Protein rotational motion in solution measured by polarized fluorescence depletion. *Biophys. J.* 50: 41–53.

Yoshida, T. M., F. Zarrin, and B. G. Barisas. 1988. Measurement of protein rotational motion using frequency domain polarized fluorescence depletion. *Biophys. J.* 54:277–288.

Zhao, L., E. Pate, A. J. Baker, and R. Cooke. 1995. The myosin catalytic domain does not rotate during the working power stroke. *Biophys. J.* 69:994–999.